139
29

ACCURACY ANALYSIS OF THE SEMI-ANALYTICAL METHOD FOR SHAPE SENSITIVITY ANALYSIS

by

Bruno Barthelemy

Dissertation submitted to the Faculty of the
Virginia Polytechnic Institute and State University
in partial fulfillment of the requirements for the degree of
Doctor of Philosophy
in
Aerospace and Ocean Engineering

APPROVED:

Raphael T. Haftka, Chairman

Eric R. Johnson

Zenon Mróz

Raymond H. Plaut

Junuthula N. Reddy

October, 1987

Blacksburg, Virginia

ACCURACY ANALYSIS OF THE SEMI-ANALYTICAL METHOD FOR SHAPE SENSITIVITY ANALYSIS

by

Bruno Barthelemy

Raphael T. Haftka, Chairman

Aerospace and Ocean Engineering

(ABSTRACT)

The semi-analytical method, widely used for calculating derivatives of static response with respect to design variables for structures modeled by finite elements, is studied in this research. The research shows that the method can have serious accuracy problems for shape design variables in structures modeled by beam, plate, truss, frame, and solid elements. Local and global indices are developed to test the accuracy of the semi-analytical method. The local indices provide insight into the problem of large errors for the semi-analytical method. Local error magnification indices are developed for beam and plane truss structures, and several examples showing the severity of the problem are presented. The global index provides us with a general method for checking the accuracy of the semi-analytical method for any type of model. It characterizes the difference in errors between a general finite-difference method and the semi-analytical method. Moreover, a method improving the accuracy of the semi-analytical method (when possible) is provided. Examples are presented showing the use of the global index.

Acknowledgements

I am much indebted to Dr. Raphael Haftka, my advisor, for his guidance and support throughout this research. His experience and knowledge were of great help in this research, and his understanding and patience made this Ph.D. and specially the end of it certainly less stressful than it is supposed to be. My gratitude is also extended to the faculty members of my doctoral committee: Dr. Eric Johnson, Dr. Zenon Mróz, Dr. Raymond Plaut, and Dr. Junuthula Reddy.

I am grateful to my wife for her constant moral support and her patience. Je voudrais aussi remercier mes parents, . Sans leur support moral et financier, je n'aurais sans doute pas entrepris des études á Virginia Tech.

I acknowledge with gratitude the source of funding for this work: NASA Langley Research Center through NASA Research Grant NAG-1-224, Ford Motor Company through a summer support at their Research Laboratories in 1985, and Virginia Polytechnic Institute and State University's Graduate School through a 1985-1986 Cunningham Fellowship.

Thanks to the past and present guys of "Femoyer Lounge" for their helps during the numerous "coffee breaks" that this research required.

Table of Contents

List of Illustrations

List of Tables

Chapter 1

Introduction

Sensitivity derivatives of objective functions and constraints are an important ingredient of most optimization algorithms. They are used for calculation of search directions and constraint approximations. In structural optimization, the constraints are typically placed on structural response such as displacements or stresses.

With advanced structural analysis programs it is now possible to evaluate structural response accurately at reasonable cost. There are many programs available on the market for this purpose, finite-element, boundary-element, shell analysis programs, each with a particular field of application. Sensitivity analysis is much less advanced. There is no general code which computes the sensitivity of structural response with respect to all variables. Moreover, the cost of sensitivity analysis can be very high, ranging from a fraction to several times the cost of one analysis for each derivative (derivative of one function with respect to one variable).

1.1 Literature Review

Interest in sensitivity analysis of structural response is evident in the large number of publications on the topic (e.g., Refs. 1,2). There are several analytical methods for calculating the sensitivity of static structural response to changes in modelling or design parameters, including direct or adjoint methods. In theory, the relative efficiency of the two approaches depends on the relative number of constraints and variables. If the number of design variables is larger than the number of the response constraints that need to be differentiated, the adjoint method can be expected to be more efficient, and vice versa. In practice, relative efficiency also depends on the software implementation. Dopker and Choi indicate in Ref. 3 that the direct formulation was more efficient than the adjoint formulation in their example when a change in a design variable modified the entire structure.

Two analytical approaches are currently used to obtain the equations for the sensitivity of structural response. One starts with the continuum equations of the structure. Haug, Choi and co-workers (Refs. 3 to 6) start with a bilinear form for the energy to obtain the continuum equations governing the sensitivity of structural response, which they solve by finite-element discretization. They attach particular importance in obtaining the sensitivity field without modifying the finite element program they use. They obtain the derivatives by postprocessing the finite-element results and by applying additional loads to the structure.

Mróz and Dems (Refs. 7,8) also use a continuum approach. They start from the principle of virtual work to derive the sensitivities of the structural response using the adjoint formulation. That approach was generalized in Refs. 9 and 10 to the direct formulation. Both the direct and adjoint formulation for sizing variables (such as cross-sectional areas of trusses, fiber orientation angles) were implemented in structural analysis programs in Ref. 11, without changing the programs (finite element and shell analysis programs), requiring only loading the structure via initial strains, initial

stresses, and body forces. However, most structural analysis packages do not have these loading capabilities.

The second approach starts with the discretized equations of the finite-element program. This approach is difficult to implement in general purpose finite-element programs, with much of the difficulty associated with obtaining analytical derivatives of the stiffness matrix. For these reasons two finite-difference approximation methods are currently popular. Overall finite difference (OFD) sensitivity calculations (where the entire analysis is repeated for a perturbed variable) are easy to implement but can be quite costly. For this reason, a semi-analytical (SA) compromise method has been gaining popularity (e.g., Refs. 12-15). The SA approach is based on a finite-difference approximation of the derivatives of the stiffness matrix followed by an analytical evaluation of response sensitivity. It is almost as easy to implement as the OFD approach and as efficient as the analytical approaches. For example, NASTRAN, a general purpose finite-element program with some sensitivity analysis capabilities (Refs. 12,13), uses this method. Both OFD and SA methods are subject to truncation and condition errors which depend on the finite-difference method, the magnitude of the step size, and machine accuracy.

The difficulties associated with obtaining analytical derivatives of the stiffness matrix are more pronounced for shape design variables than for section variables. Therefore, the SA approach is often used for shape design sensitivity (e.g., Refs. 15,16). However, the superior efficiency of the SA method as compared to OFD may be accompanied by increased truncation errors. The problem of high truncation errors was first encountered for a beam model of a car structure in Ref. 17. To check whether the problem was associated with the complexity of the car structure, a simple cantilever beam was analyzed, and the same accuracy problem was encountered.

Refs. 18 and 19 present methods to find step sizes which minimize the total error. However, these methods require computation of the approximate derivatives several times and are too costly to use in structural optimization.

1.2 Objectives and Outline

The purpose of this work is to analyze and characterize the errors for the derivatives using the SA method for shape variables. In this work, we assume the SA and OFD methods use forward-finite-differences in their approximations.

Chapter 2 presents different problems for which the SA method fails to obtain accurate derivatives. The structures analyzed are made of truss, beam, plate, frame, and solid elements, emphasizing that the error problem of the SA method is not particular to beam elements (Refs. 17,20). It will be shown that the reason for the large truncation error in the SA method is that the derivatives of the displacement field often do not form a compatible field for the structure.

In Chapter 3, local indices are presented for the beam and truss elements. These indices show that the large errors of the SA method are a function of the ratio of rigid body rotations to elastic deformations as well as the ratio (for the truss index) of the rotation of the local axis of the element to the extension of the element due to a change in the shape variable. These indices give us insight into the problem, as well as quick identification of cases where large errors are to be expected.

In Chapter 4, we present a global index characterizing the accuracy of the SA method for any structure. This index is based on the computation of the relative error of the SA derivatives of the strain energy with respect to the OFD derivatives. The cost of this index is of the same order of magnitude as the cost of one derivative using the SA method. Moreover, this method provides a mechanism that can, in some instances, increase the accuracy of the SA derivatives.

Chapter 2

Accuracy Problems of the SA Method

2.1 Displacement Derivatives

Using the finite element method, we write the equilibrium equations as

$$\mathbf{K}\mathbf{u} = \mathbf{p} \tag{2.1}$$

where $\mathbf{K}$ is the stiffness matrix, and $\mathbf{u}$ and $\mathbf{p}$ are the nodal displacement and load vectors, respectively. Solving Eq. 2.1 for $\mathbf{u}$, we get

$$\mathbf{u} = \mathbf{K}^{-1}\mathbf{p} \tag{2.2}$$

Eq. 2.2 employs for convenience the inverse of $\mathbf{K}$, but for the actual computations $\mathbf{K}$ is factored rather than inverted. To obtain the derivative of $\mathbf{u}$ with respect to a variable s , we differentiate Eq. 2.2:

$$\frac{d\mathbf{u}}{ds} = \frac{d(\mathbf{K}^{-1}\mathbf{p})}{ds} \tag{2.3}$$

Eq. 2.3 is not convenient for analytical calculations, but forms the basis for the OFD approach. That is,

$$\frac{\mathbf{du}}{ds} \cong \frac{\Delta(\mathbf{K}^{-1}\mathbf{p})}{\Delta s} \equiv \left[\frac{\Delta \mathbf{u}}{\Delta s}\right]_{ofd} \tag{2.4}$$

where $\frac{\Delta f}{\Delta s}$ denotes a finite-difference approximation to the derivative $\frac{df}{ds}$ of a function f. In this work, two such approximations are employed, the forward-difference approximation

$$\frac{df}{ds} \cong \left[\frac{\Delta f}{\Delta s}\right]^{FD} = \frac{f(s + \Delta s) - f(s)}{\Delta s} \tag{2.5}$$

and the central-difference approximation

$$\frac{df}{ds} \cong \left[\frac{\Delta f}{\Delta s}\right]^{CD} = \frac{f(s + \Delta s) - f(s - \Delta s)}{2\Delta s} \tag{2.6}$$

The OFD method, Eq. 2.4, is easy to implement in a finite element program, requiring only the repeated solution of Eq. 2.1 to obtain $\mathbf{K}^{-1}\mathbf{p}$, but it is quite costly when derivatives with respect to many design parameters are needed, and when the problem size is large.

Alternatively, we can obtain the derivatives of **u** with respect to s analytically by differentiating Eq. 2.1:

$$\mathbf{K}\frac{\mathbf{du}}{ds} = \frac{\mathbf{dp}}{ds} - \frac{\mathbf{dK}}{ds}\mathbf{u} \equiv \mathbf{p}_{ps} \tag{2.7}$$

where $\mathbf{p}_{ps}$ is called the pseudo or virtual load. For future discussion, it is useful to characterize $\mathbf{p}_{ps}$ as the load that must be applied to the structure so that the resulting displacement field will be equal to $\frac{\mathbf{du}}{ds}$. Solving Eq. 2.7 for $\frac{\mathbf{du}}{ds}$ is typically inexpensive, because the matrix **K** is available in factored form from the solution of the equations of equilibrium, Eq. 2.1. However, the analytical calculation of $\frac{\mathbf{dp}}{ds}$ and $\frac{\mathbf{dK}}{ds}$ is often cumbersome and difficult to implement. The SA method combines the efficiency of the analytical approach with the easy implementation of the OFD approach by approximating Eq. 2.7 as

$$\frac{du}{ds} \cong K^{-1}\left[\frac{\Delta p}{\Delta s} - \frac{\Delta K}{\Delta s}u\right] \equiv \left[\frac{\Delta u}{\Delta s}\right]_{sa} \qquad 2.8$$

The use of a forward-difference scheme in Eq. 2.4 requires one assembly and one factorization of the stiffness matrix for each derivative, whereas Eq. 2.8 only requires assembly of the stiffness matrix for each derivative. For N variables, the use of the SA method saves N factorizations. In addition, the SA method requires the assembly of only the part of the stiffness matrix that is affected by s.

2.2 Strain-Energy Derivatives

The strain energy V of the structure is given as

$$V = \frac{1}{2}u^T K u = \frac{1}{2}p^T u \qquad 2.9$$

and its derivative

$$\frac{dV}{ds} = \frac{1}{2}\frac{du^T}{ds}p + \frac{1}{2}u^T\frac{dp}{ds} \qquad 2.10$$

We can express the SA and OFD approximation as

$$\frac{dV}{ds} \cong \left[\frac{\Delta V}{\Delta s}\right]_a = \frac{1}{2}\left[\frac{\Delta u^T}{\Delta s}\right]_a p + \frac{1}{2}u^T\frac{\Delta p}{\Delta s} \qquad 2.11$$

where the subscript a stands for either SA or OFD. Eq. 2.11 can be simplified for the SA method as

$$\left[\frac{\Delta V}{\Delta s}\right]_{SA} = -\frac{1}{2}u^T\frac{\Delta K}{\Delta s}u + u^T\frac{\Delta p}{\Delta s} \qquad 2.12$$

2.3 Truncations and Condition Errors

The error e in a forward-difference approximation is

$$e \equiv \frac{\Delta f}{\Delta s} - \frac{df}{ds} \qquad 2.13$$

The error is composed of a truncation error e_t due to a truncation of the Taylor series expansion and a condition error e_c due to errors in the computation of f (algorithmic and round-off). For a forward-difference approximation

$$e_t = \frac{\Delta s}{2}\frac{d^2 f}{ds^2}(s + \eta\Delta s) \qquad 0 \leq \eta \leq 1 \qquad 2.14$$

That is, the truncation part of the forward-difference error is proportional to the second derivative of f at a point between s and s + Δs , and to the step size Δs.

As the condition error e_c is roughly proportional to $\frac{1}{\Delta s}$, we face the so called step-size dilemma. If Δs is too large we have a large truncation error, while if Δs is too small the condition error can become excessive. Fig. 1 presents a typical plot of the errors e for a function f versus the step size, with e_{min} being the minimum errors that we can obtain using the forward-finite difference approximation. If e_{min} is smaller than e_{accept}, an acceptable level of error, then there is a step size range (between Δs_{min} and Δs_{max}) that will yield an error less than e_{accept}. In the worst situation, e_{accept} is smaller than e_{min} and no step size will be acceptable.

Both the SA and OFD methods suffer from truncation and condition errors. Chapters 3 and 4 investigate the large truncation errors encountered in the SA method.

2.4 Car Example

The problem of occasional high truncation errors of the SA method was first encountered with a stick model of a car structure shown in Fig. 2. The model is made of about 300 beam elements and contains around 300 nodes with 6 degrees of freedom per node. The derivatives of the strain energy were computed with respect to some stiffness variables (cross-sectional areas, moments of inertia, torsional constants) and some global dimensions of the model (shape variables). The dimensions defined key lengths, widths, and heights of the car, with the length dimensions shown in Fig. 3. The car was loaded by point forces applied to the front wheels' axle, the rear wheels' axle being fixed. The EAL (Engineering Analysis Language, Ref. 21) program was used for the analysis and sensitivity calculations. Originally, the OFD method was used to compute these derivatives, and in order to make the computation more efficient, the SA method was implemented.

The SA method was first implemented for the calculation of the derivatives of the strain energy of the model with respect to stiffness variables. Because each stiffness variable controlled only a few elements, Eq. 2.12, required the assembly of only a small part of the stiffness matrix. The strain energy derivatives with respect to 300 variables were computed, and the SA method proved to be 80% faster than the OFD method. The accuracy of the SA method was very good because the beam stiffness matrix is a linear function of the cross-sectional variables used.

The SA method was then implemented for shape variables. The dependence of the stiffness matrix on these shape variables is very complex, and the entire stiffness matrix had to be assembled for each derivative. This resulted in a smaller saving (70%) over the OFD method than for stiffness variables.

For some shape variables the method proved to be very sensitive to the step size, and in some cases no step size gave accurate derivatives. Fig. 4 presents the relative error in the derivative of the strain energy with respect to one of the length variables as a function of the relative step size. All the data

points below the solid line have an error smaller than 1%. The exact derivative was estimated using higher order approximations.

The results, typical of all the derivatives tested, show three characteristics. For large step sizes (relative step size larger than 10^{-6}), the OFD method has a smaller error (mostly truncation error) than the SA method. The step-size range for which the approximate derivative has an error less than 1% is much larger for the OFD than for the SA approximation, and for small step sizes, the OFD method has a larger error (mostly condition error) than the SA method. Fig. 4 shows that for a relative step size of 10^{-7} the SA method approximates the derivative well. For some variables, however, no step size giving accurate derivatives could be found!

In order to solve the accuracy problem, a central-difference approximation was used for the stiffness matrix derivatives. Fig. 5 presents comparison between forward- and central-difference approximations using the SA method for one of the length variables. For this variable, the error in the forward-difference SA method was always larger than 10%. However, the SA method using the more expensive central-difference scheme gave satisfactory accuracy for all variables. The computational savings of the SA method using a central-difference scheme versus the OFD method dropped to 50%, instead of the original 70% savings.

2.5 Beam and Plate Elements

Because the stick model of the car is complex, the accuracy problem of the SA method was further investigated for simple beam models. The purpose of these simple examples was to determine whether the large errors encountered for the stick model were associated with the complexity of the model or were inherent to shape derivatives of structures modeled with beam elements (see Ref. 20). As an example, consider a cantilever beam with uniform rigidity EI and length L under a tip moment M (Fig. 6). Errors in the derivatives of the tip displacement with respect to the beam

length using both the SA and OFD methods for finite element models consisting of 1 to 20 beam elements are presented in Fig. 7. The SA method diverges, whereas the OFD errors are small and do not depend on the number of elements.

The cause for the large truncation error is that the derivative $\frac{du}{dL}$ of the displacement field of a beam structure with respect to a geometry parameter is not a legitimate beam displacement field, in that the nodal rotations $\frac{d\theta}{dL}$ do not correspond to the slope of the nodal displacements $\frac{dw}{dL}$. Indeed, the vertical displacement, w, and the rotation of the cross section, θ, are

$$w = \frac{M}{2EI}x^2 \qquad 2.15$$

$$\theta = \frac{M}{EI}x \qquad 2.16$$

If we assume that with a change in length all points on the beam stretch or shrink uniformly, x the axial coordinate of the beam is $x = \xi L$ where ξ is invariant under changes in length. The displacements and rotations are written as

$$w = \frac{M}{2EI}\xi^2 L^2 \qquad 2.17$$

$$\theta = \frac{M}{EI}\xi L \qquad 2.18$$

Differentiating Eqs. 2.17 and 2.18 with respect to L, we get

$$\frac{dw}{dL} = \frac{M}{EI}\xi^2 L = \frac{M}{EI}\frac{x^2}{L} \qquad 2.19$$

$$\frac{d\theta}{dL} = \frac{M}{EI}\xi = \frac{M}{EI}\frac{x}{L} \qquad 2.20$$

and while $\theta = \frac{dw}{dx}$, the relation between the vertical displacement and rotation of the cross section for the displacement derivatives (Eqs. 2.19 and 2.20) is

$$\frac{d\theta}{dL} = \frac{1}{2}\frac{d}{dx}\left[\frac{dw}{dL}\right] \qquad 2.21$$

so that the derivatives of the displacement and rotations in Eqs. 2.19 and 2.20 do not describe a possible beam displacement field. This means that there is no physical field of applied loads that can produce a continuous displacement and rotation field equal to $\frac{dw}{dL}$ and $\frac{d\theta}{dL}$.

For any finite-element mesh, it is possible to apply nodal forces and moments (pseudo load $\mathbf{p}_{ps}$) so as to obtain the correct values of $\frac{dw}{dL}$ and $\frac{d\theta}{dL}$ at the nodes only; but as the mesh is refined the discrepancy between displacements and rotations forces higher and higher local curvature. This is shown in Fig. 8 which presents a plot of the curvature of $\frac{dw}{dL}$. The curvature, normalized with respect to its maximum value for the single element model, is plotted for three discretizations of the beam (1, 2, and 5 elements).

The pseudo load $\mathbf{p}_{ps}$, needed to make the structure deform into $\frac{du}{dL}$ and producing these high curvatures, consists of nodal forces and moments that tend to cancel each other, and that change with mesh refinement. Fig. 9 shows the bending moment at the root due to the pseudo load normalized by the root bending moment (due to the pseudo load) for a one-element model versus the number of elements in the model. Clearly the root-bending moment diverges with an increasing number of elements. As the energy stored in the beam due to the pseudo load increases, small truncation errors in $\mathbf{p}_{ps}$ induced by the finite difference approximation are magnified into large errors in $\left[\frac{\Delta u}{\Delta s}\right]_{ss}$.

The same type of problem can be expected for plate problems when Kirchhoff plate theory is used. The rotations are the slopes of the displacements, and $\frac{du}{ds}$ may violate that relation. As an example consider a square plate, clamped at all edges and subjected to a point load at the middle (Fig. 10). The derivative of the vertical displacement under the load with respect to the side length was computed for different finite-element models (from 2×2 to 20×20 elements for a one-quarter plate model). Fig. 11 presents the OFD and SA approximations' errors (for a step size of 1 percent)

versus the number of elements in the finite-element model. The SA errors diverge as for the beam example, whereas the OFD errors again are constant for the different models.

2.6 Incompressibility

The problem of $\frac{du}{ds}$ being incompatible with the structural model is not limited to beam or plate problems, but can occur when the material is incompressible or almost so. If $\frac{du}{ds}$ is not an incompressible field we can expect problems for the SA method. Consider for example, a slab in tension made of incompressible material (Poisson's ratio $\nu = 0.5$) shown in Fig. 12. For the boundary conditions described in Fig. 12, the axial (u) and transverse (v, w) displacements are

$$u = \frac{P}{EA}x \tag{2.22}$$

$$v = -\nu\frac{P}{EA}y \qquad w = -\nu\frac{P}{EA}z \tag{2.23}$$

where A is the cross-sectional area. The derivative of this displacement field with respect to the length L , assuming as in the beam case that $x = \xi L$ where ξ is invariant under changes in length, will be

$$\frac{du}{dL} = \frac{d}{dL}\left[\frac{P}{EA}\xi L\right] = \frac{P}{EA}\xi = \frac{P}{EA}\frac{x}{L} \tag{2.24}$$

$$\frac{dv}{dL} = \frac{dw}{dL} = 0 \tag{2.25}$$

This sensitivity field, if treated as a displacement field, is not incompressible. With the material being incompressible, it is impossible to impose this displacement field on the structure. Fig. 13 presents the errors of the SA and OFD methods for the derivative of the strain-energy with respect to L versus Poisson's ratio ν (for a step-size of 1 percent). We see that as ν approaches incompressibility the SA method diverges, producing very large errors.

2.7 Beam-Like Structures

When a beam-like structure is modeled by elements which are not restricted to beam theory, it may seem that we should not encounter the same accuracy problem. Indeed, in this case there is no divergence with mesh refinement. However, for a structure with one or two dimensions which are much smaller than the third dimension, severe errors in the SA method are encountered for bending loads, because it is extremely difficult to impose on beam-like structures a displacement field that is grossly incompatible with beam theory. The difficulty increases with the aspect ratio of the structure and so does the error.

For beam theory, we usually neglect shear deformations, because the ratio of shear energy to bending energy tends to zero as the beam aspect ratio increases. Indeed, considering a cantilever beam, with a cross-sectional area of unit width and height H, under a tip vertical force (see Fig. 14-a), the displacement field, for a Poisson's ratio $\nu = 0$, is

$$u = -\frac{P}{EI}\left[Lxy - x^2\frac{y}{2} + H^2\frac{y}{4} - \frac{y^3}{3}\right] \qquad 2.26$$

$$v = \frac{P}{EI}\left[L\frac{x^2}{2} - \frac{x^3}{6}\right] \qquad 2.27$$

where $I = \frac{H^3}{12}$. The corresponding strain field is

$$\varepsilon_x = -\frac{P}{EI}[Ly - xy] \qquad 2.28$$

$$\varepsilon_y = 0 \qquad 2.29$$

$$\gamma_{xy} = \frac{P}{EI}\left[-\frac{H^2}{4} + y^2\right] \qquad 2.30$$

and the bending and shear energies (V_b, V_s) are

$$V_b = \frac{E}{2}\int \varepsilon_x^2 dV = \frac{P^2}{2EI}\frac{L^3}{3} \qquad 2.31$$

$$V_s = \frac{G}{2}\int \gamma_{xy}^2 dV = \frac{P^2}{2EI}\frac{LH^2}{5} \qquad 2.32$$

The ratio of shear to bending energies is then

$$R = \frac{3}{5}\frac{H^2}{L^2} \qquad 2.33$$

Assuming (as in the preceding examples) that all points on the beam stretch uniformly as the beam length changes ($x = \xi L$), the derivative of the displacement field Eqs. 2.26 and 2.27 is

$$\frac{du}{dL} = -\frac{P}{EI}\left[2xy - x^2\frac{y}{L}\right] \qquad 2.34$$

$$\frac{dv}{dL} = \frac{P}{EI}\left[\frac{3}{2}x^2 - \frac{x^3}{2L}\right] \qquad 2.35$$

Following the same procedure used for the displacement field, the ratio of energies corresponding to the derivative of the displacement field is

$$\dot{R} = \frac{3}{5}\frac{L^2}{H^2} \qquad 2.36$$

This shows that under the pseudo load, the beam will be forced to deform in a mode dominated by shear rather than by bending. Beams are very stiff in shear and very flexible in bending. If in the approximation of the pseudo-load vector some errors are made transforming shear loads into bending loads, the resulting displacement field will be greatly affected. Moreover, this situation will worsen as the aspect ratio of the beam is increased.

Plane Stress Elements This is first demonstrated for a beam modeled by plane stress elements (Fig. 14-b). In the analytical solution, the boundary conditions are chosen so as to obtain a solution to

the differential equation in u and v; they are $u = v = \frac{dv}{dx} = 0$ for $x = y = 0$ (see Ref. 22). However, we cannot apply exactly these boundary conditions on the finite-element model. Even though, the boundary conditions for the finite-element method (see Fig. 14-b) are different, the corresponding displacement field is very close to the analytical solution. The derivatives of the tip displacement with respect to the length were calculated for a fixed height and an aspect ratio varying from 10 to 50. Each model contained 20 triangular elements through the height, H, with a constant element aspect ratio of 1, so that the total number of elements was varied from 4000 to 20000. Fig. 15 presents the results for the SA and OFD errors (for a step size of 1 percent) versus the beam aspect ratio, and shows that the errors of the SA method increase sharply with the beam aspect ratio.

Truss Elements Next we analyze a truss beam (Fig. 16) composed of square cells each containing 5 truss elements. The number of cells was varied from 1 to 20, changing the beam aspect ratio from 1 to 20. The errors of the SA and OFD approximations of the strain-energy derivatives (for a step size of 1 percent) are plotted versus the beam aspect ratio (Fig. 17). They show behavior similar to that of the plane stress beam.

Solid Elements The SA and OFD methods applied to beams modeled by solid elements displays similar behavior. Fig. 18 presents a cantilever beam made out of solid elements subjected to tip loading. The model contains one element through the section, and the aspect ratio of the elements is 1 (width to length and width to height). The number of elements in the models along the length was varied from 1 to 20. The errors of the SA and OFD approximations of the strain energy derivatives with respect to the beam length (for a step size of 1 percent) are plotted versus the beam aspect ratio (Fig. 19).

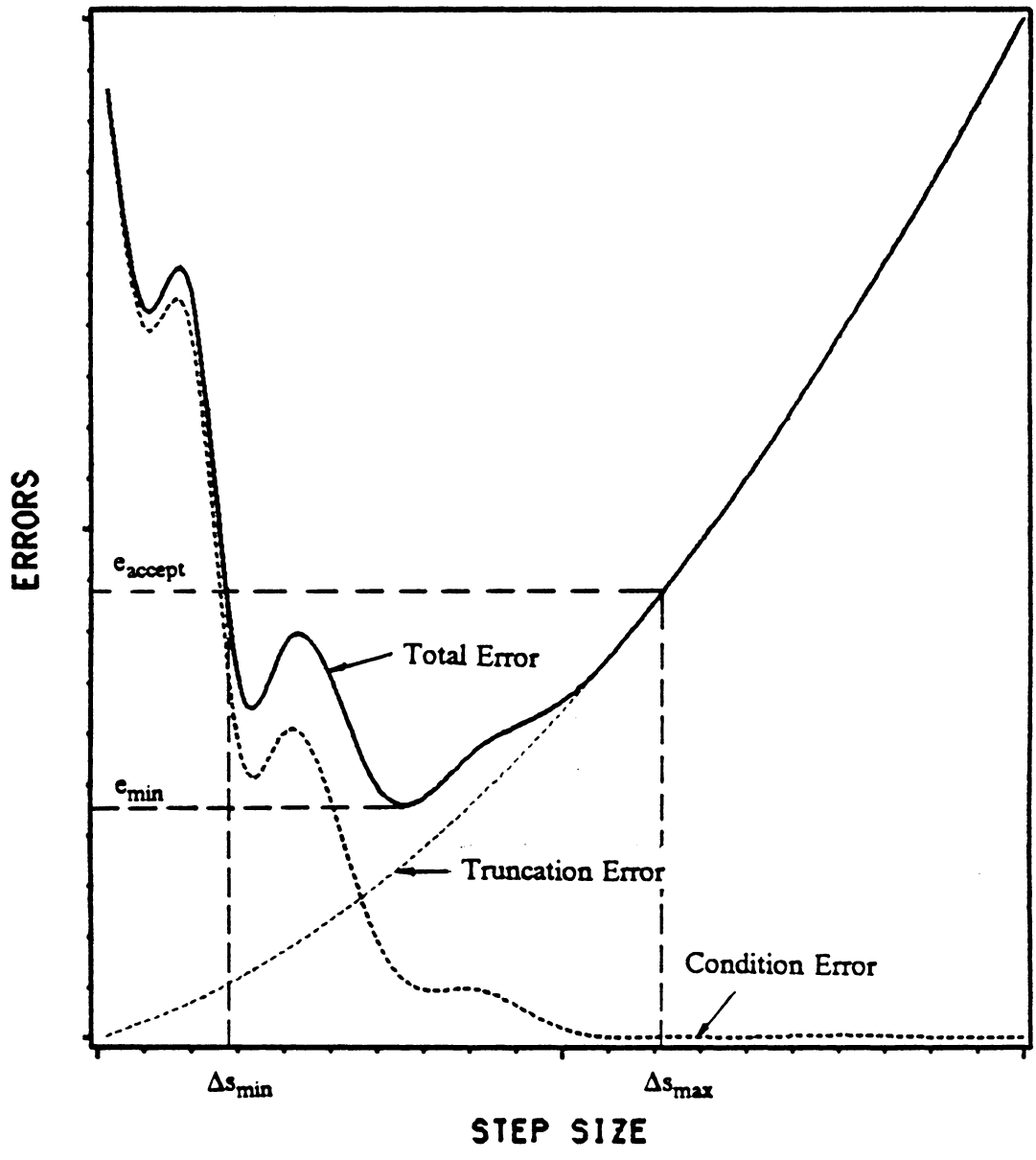

Figure 1. Typical errors in finite-difference approximation

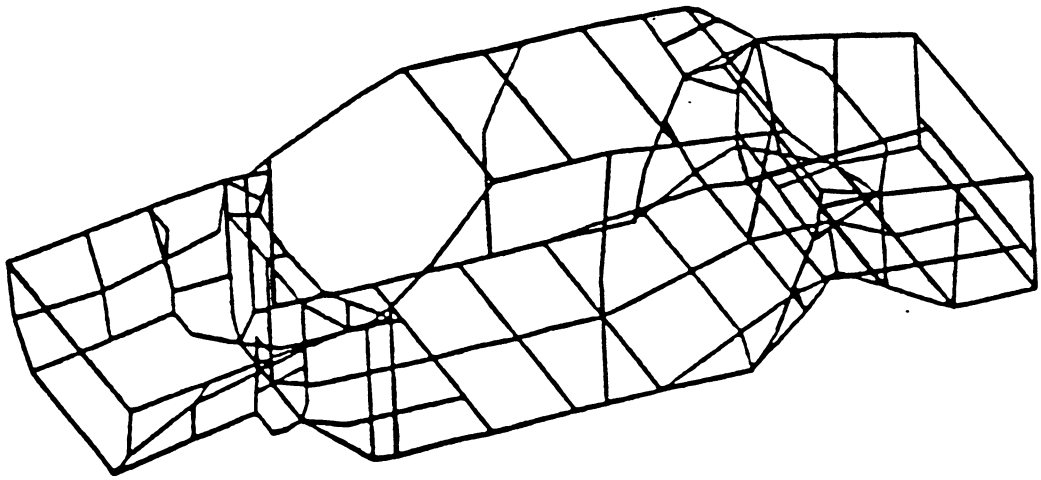

Figure 2. Stick model of a vehicle structure

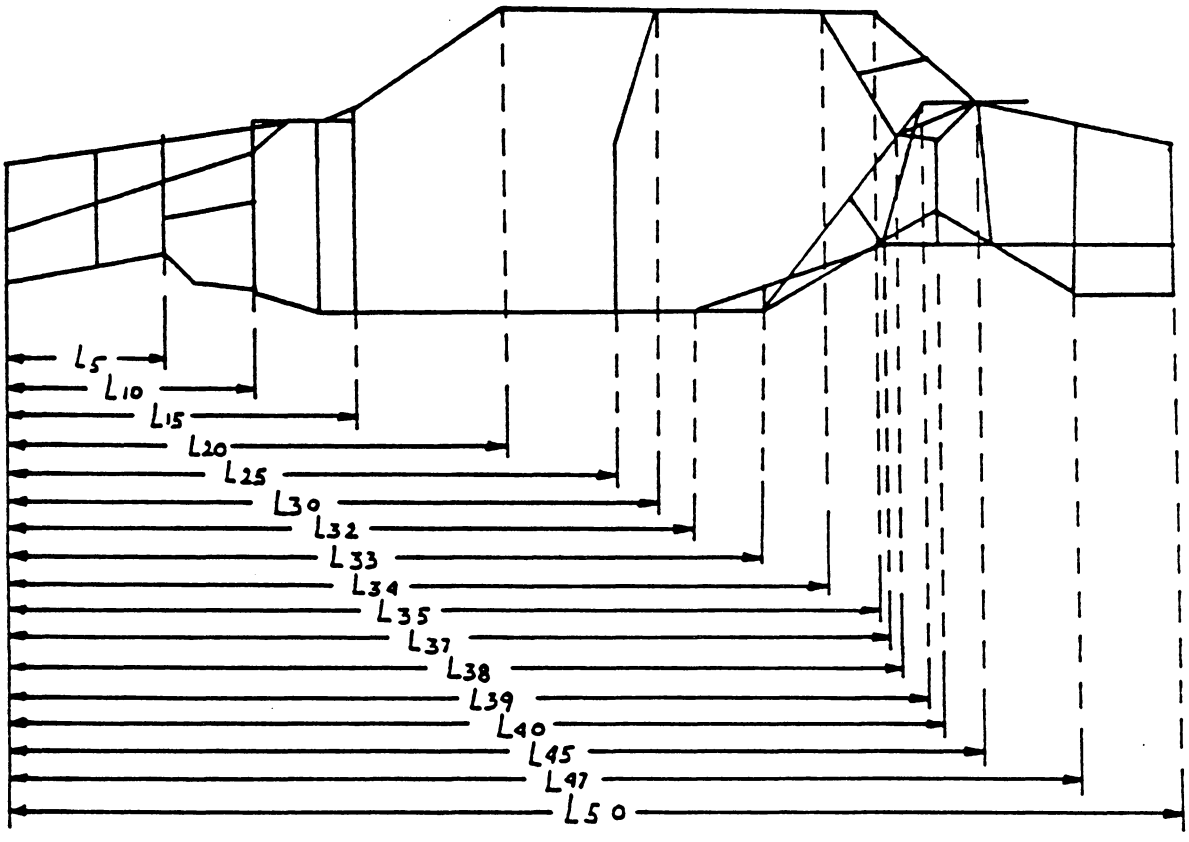

Figure 3. Definition of length dimensions for generic stick model of a car

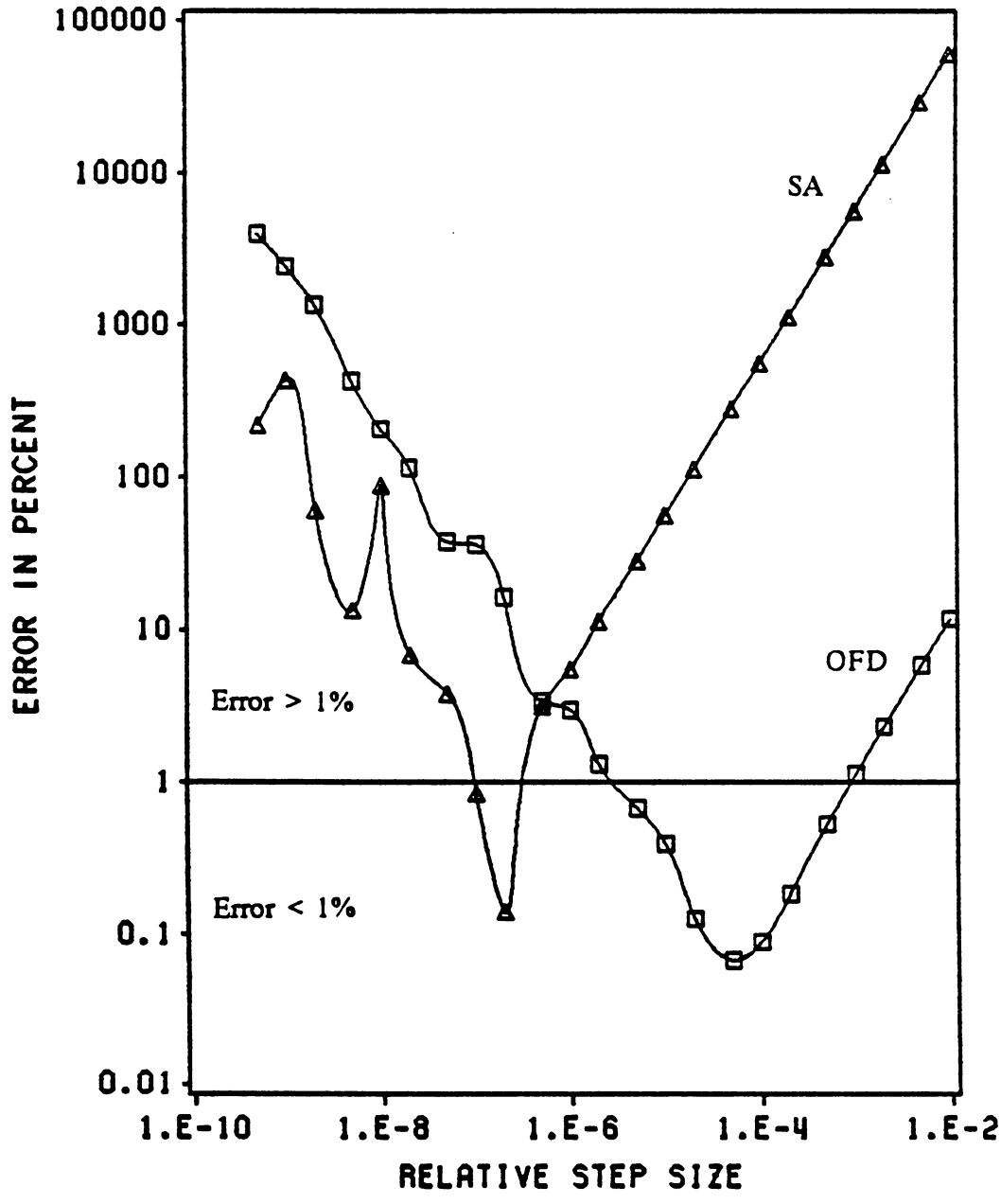

Figure 4. Errors in strain-energy derivative with respect to a length dimension of stick model for the OFD and SA methods

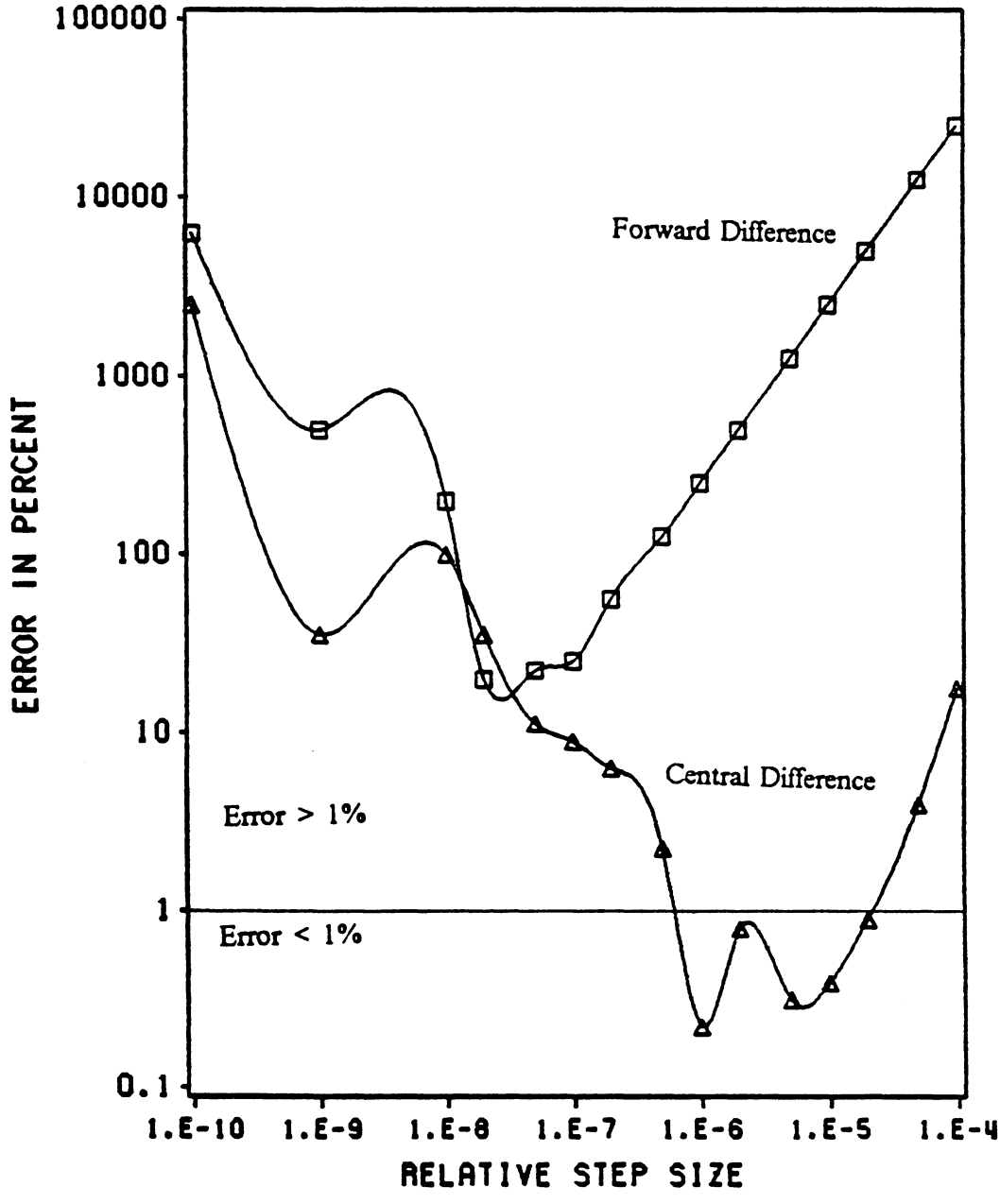

Figure 5. Forward- and central-difference SA approximations of the derivative of the strain energy with respect to a second length variable for stick model

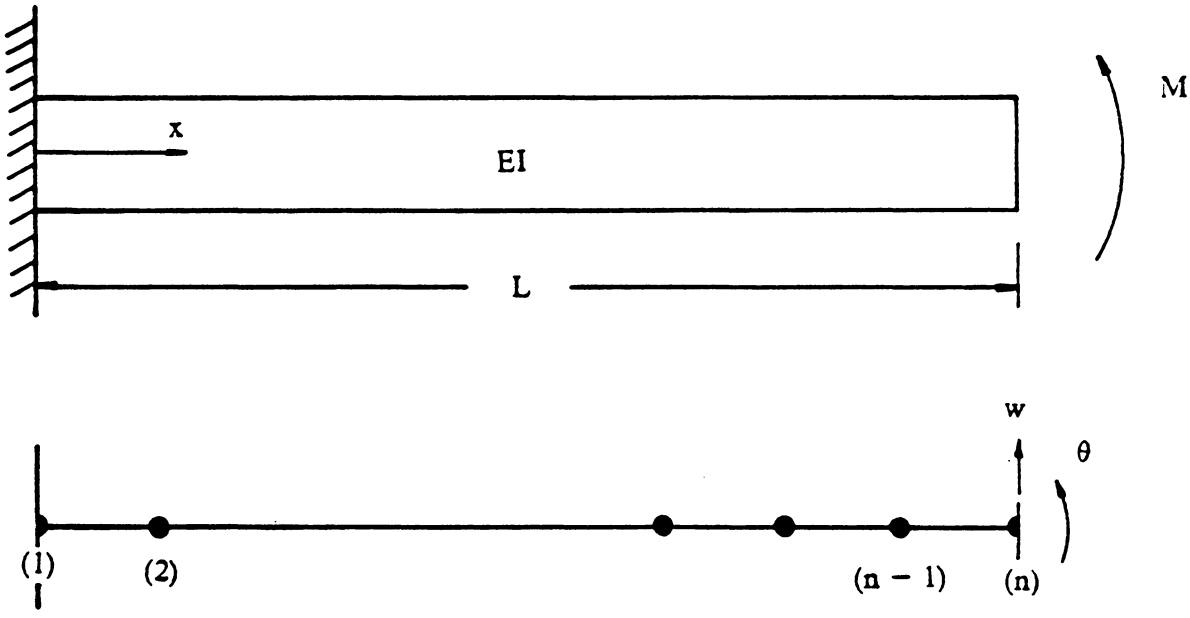

Figure 6. Geometry, loading, and discretization for cantilever beam

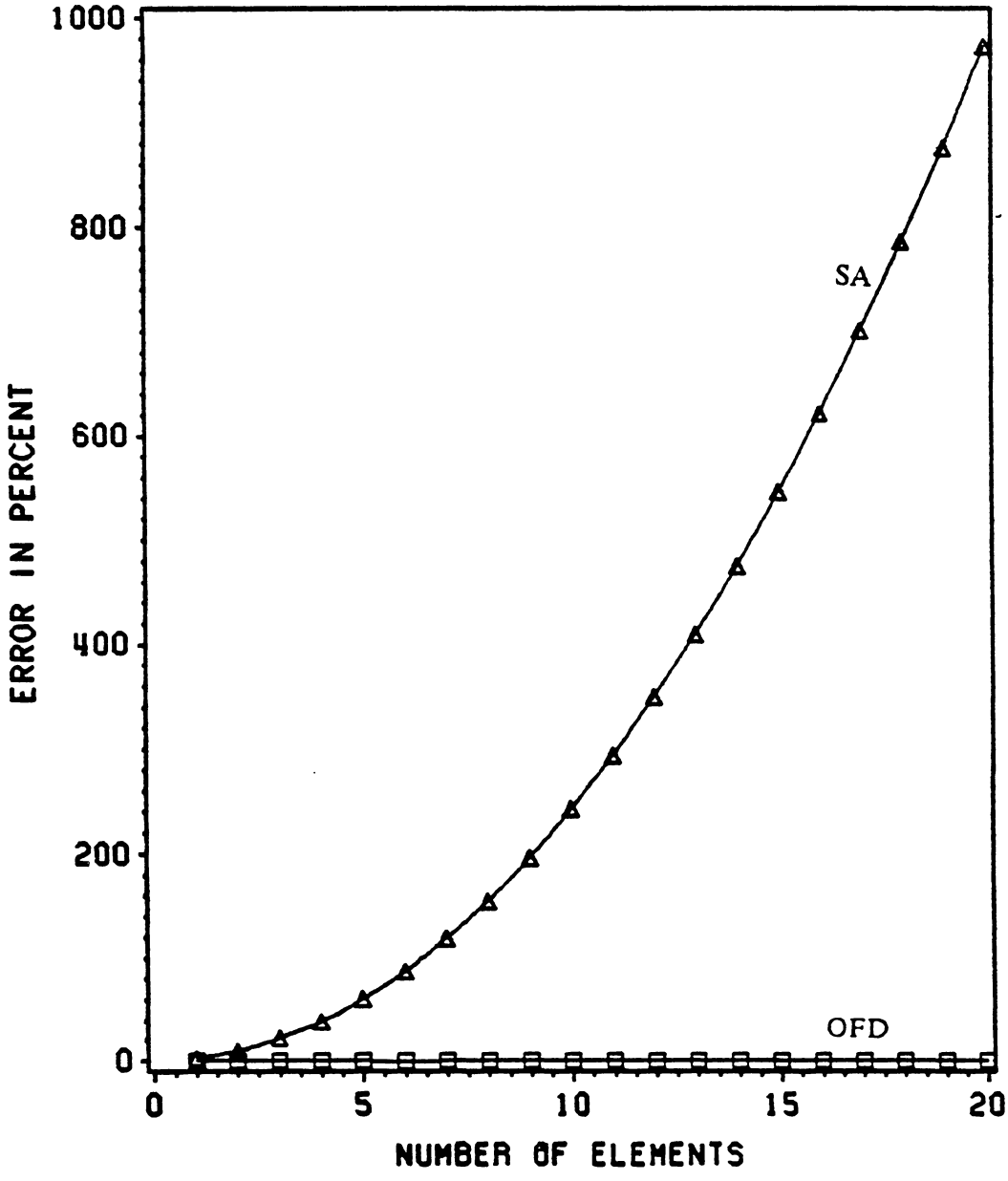

Figure 7. Errors in the SA and OFD approximations for the derivative of vertical tip displacement with respect to length of beam modeled with beam elements (step size 1 percent)

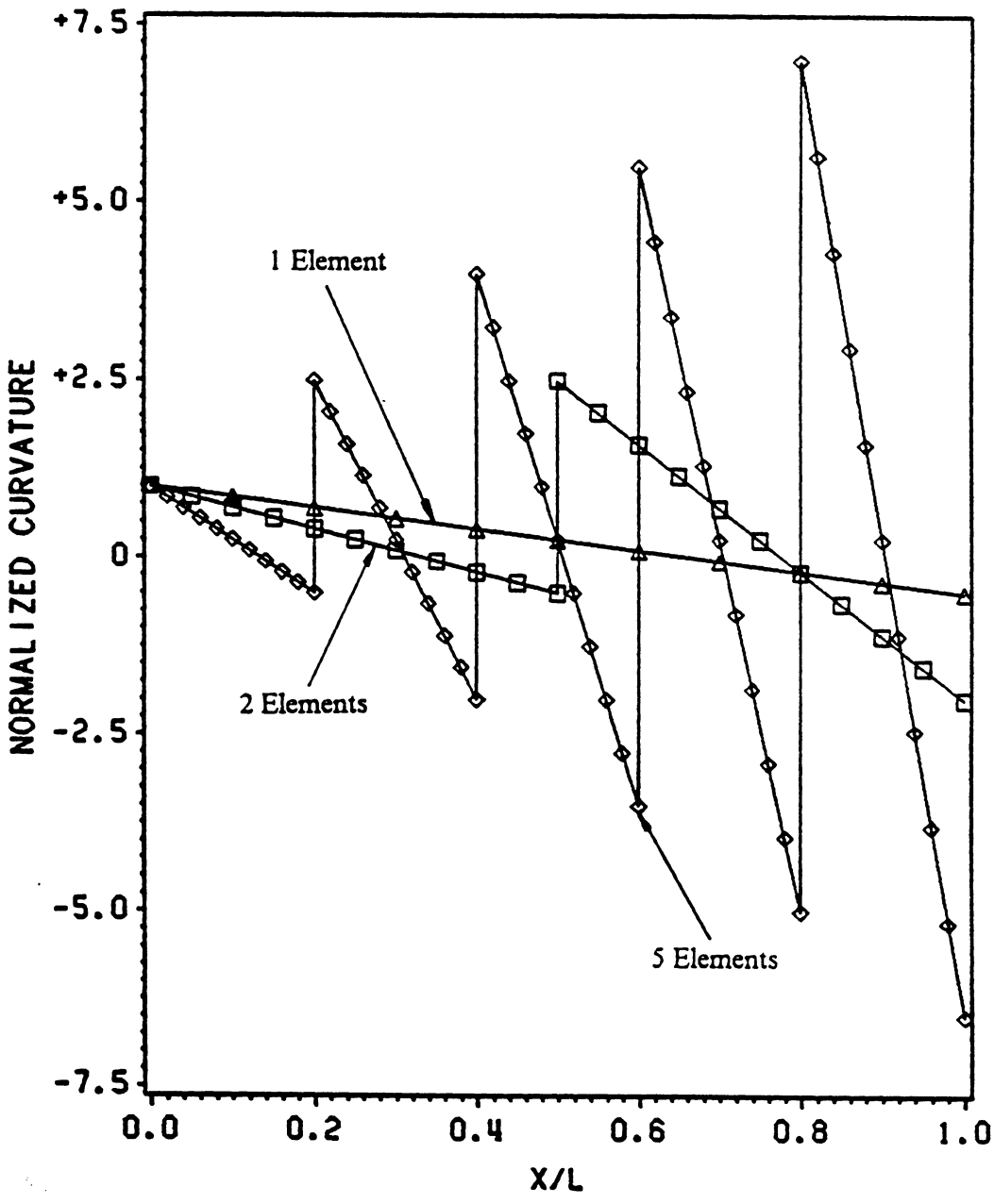

Figure 8. Curvature (normalized by maximal curvature for one element) computed from the derivatives of displacement with respect to length of cantilever beam (end moment loading)

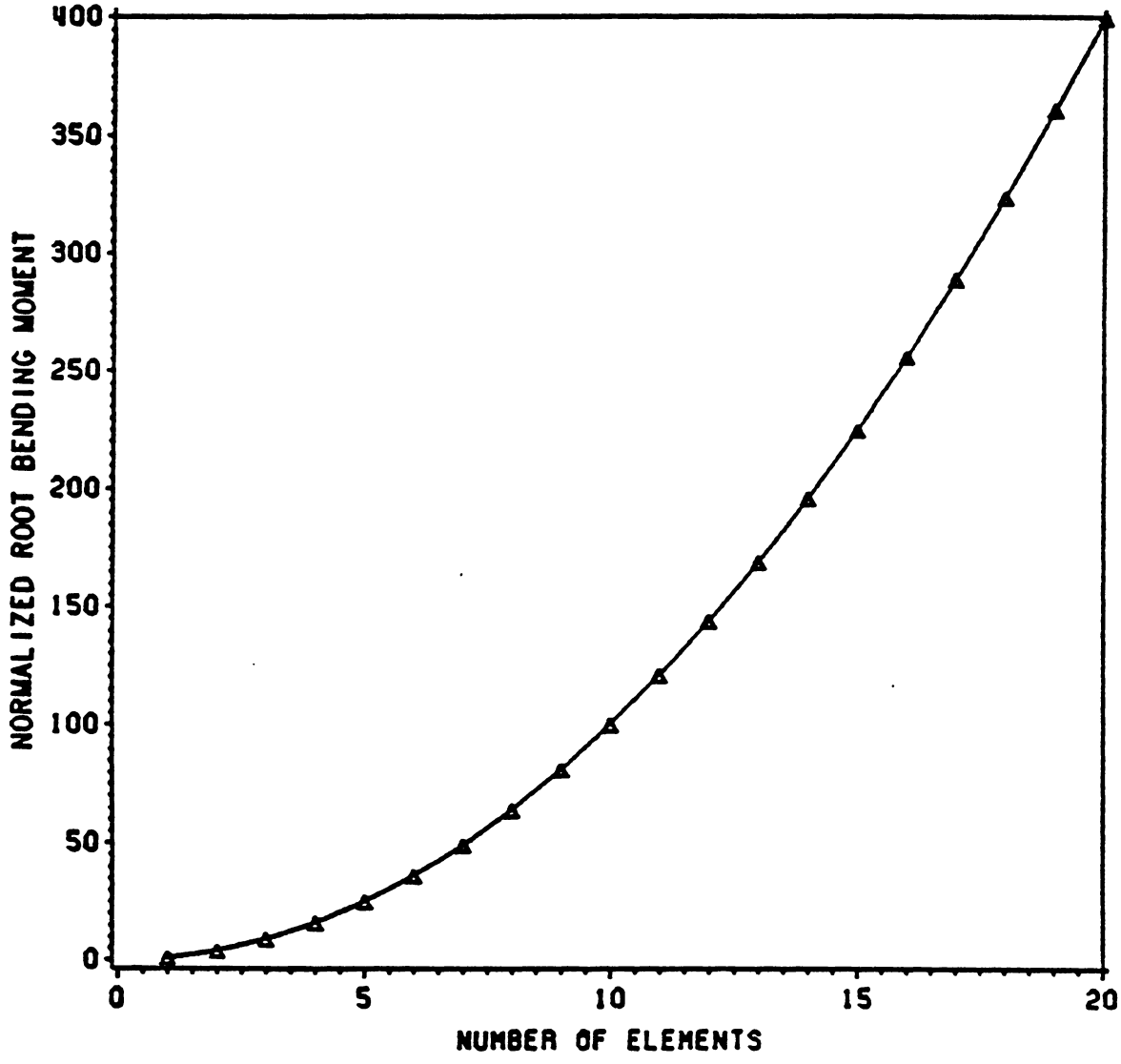

Figure 9. Bending moment at root (normalized by root moment for one element model) due to pseudo-load vector for cantilever beam under end moment

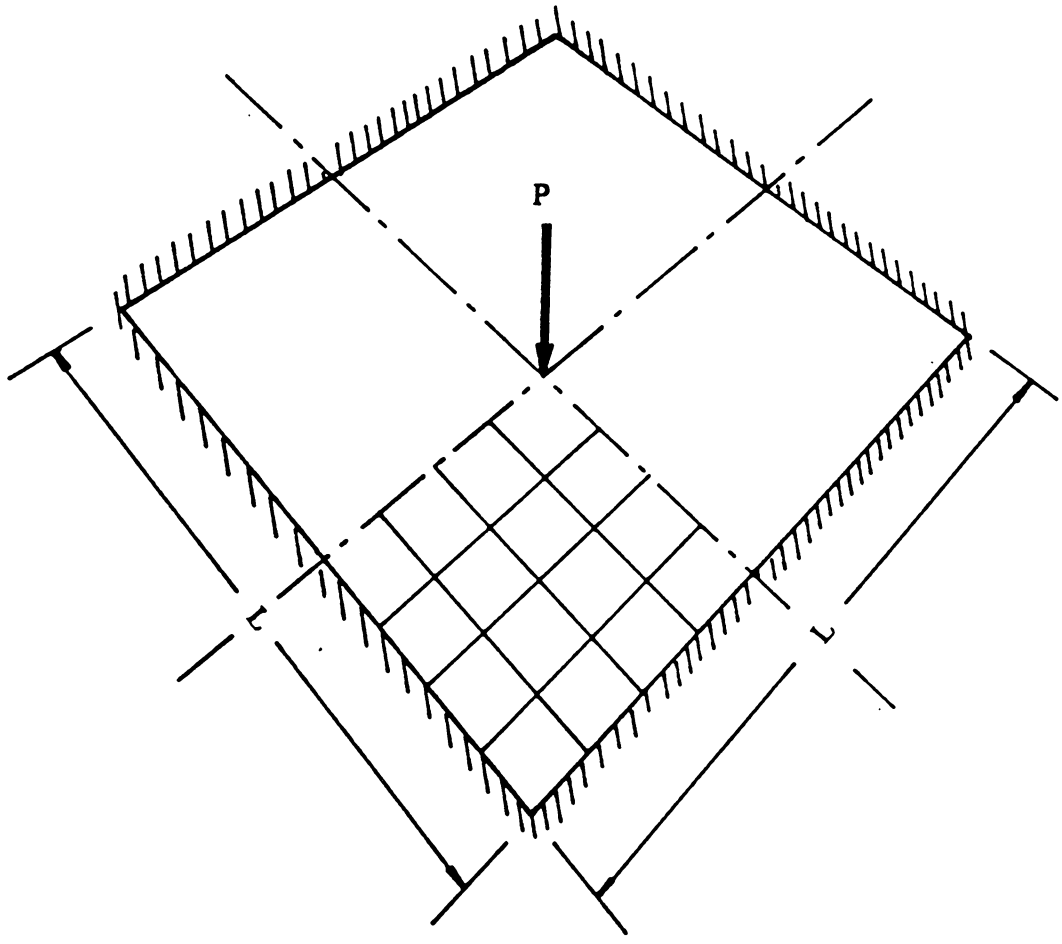

Figure 10. Geometry, loading, and finite-element model of square plate example

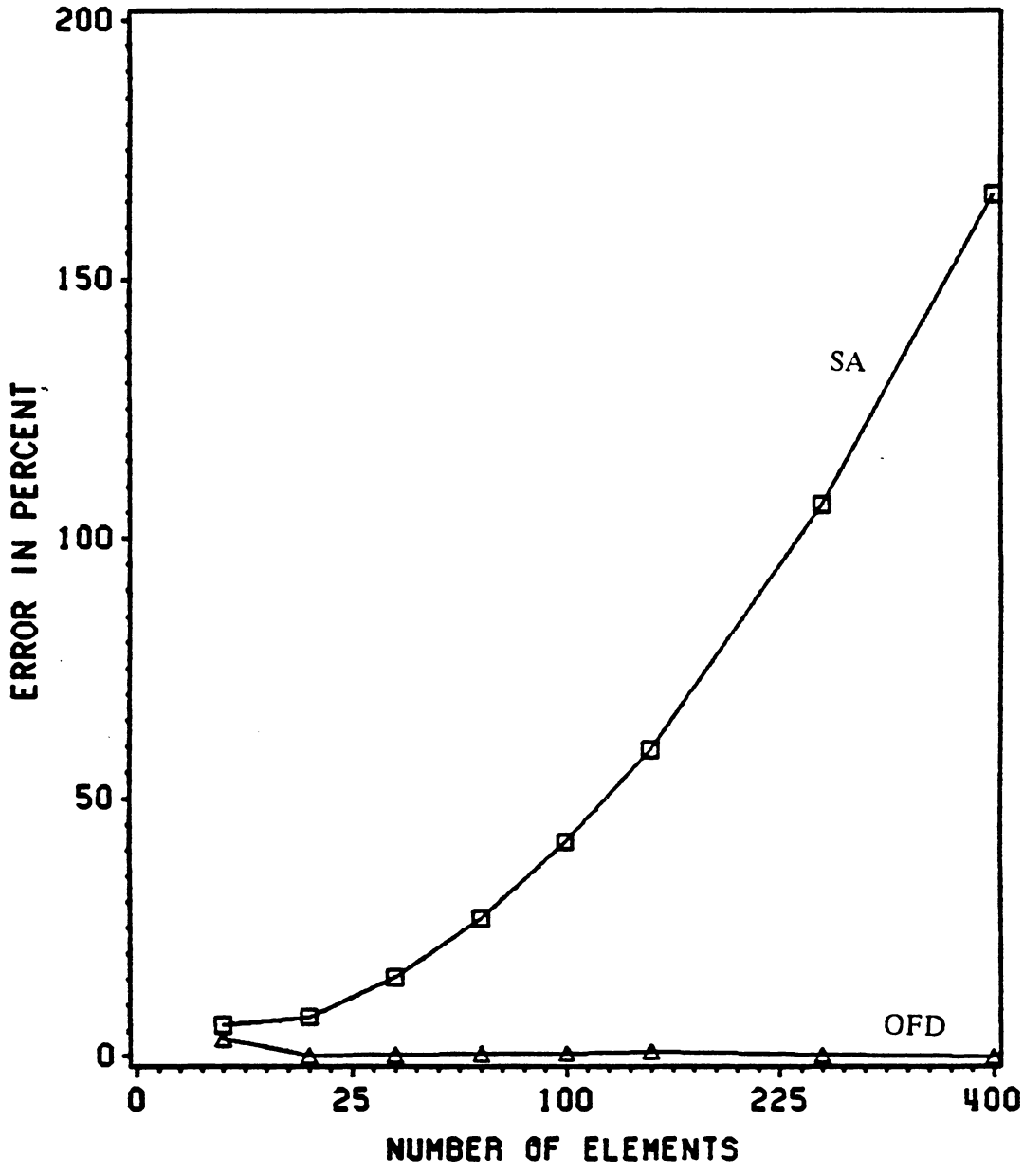

Figure 11. Errors in the SA and OFD approximations for the derivative of vertical displacement under the load with respect to side length for square plate (step size 1 percent)

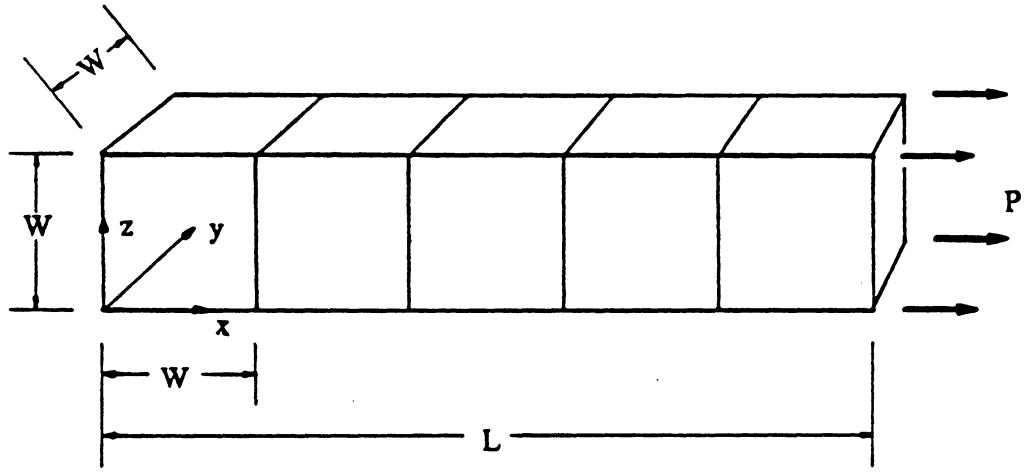

$$\frac{L}{W} = 5$$

Boundary Conditions:

Planes of symmetry x = 0, y = 0, and z = 0

Figure 12. Geometry, loading, and finite-element model of an incompressible slab modeled by solid elements

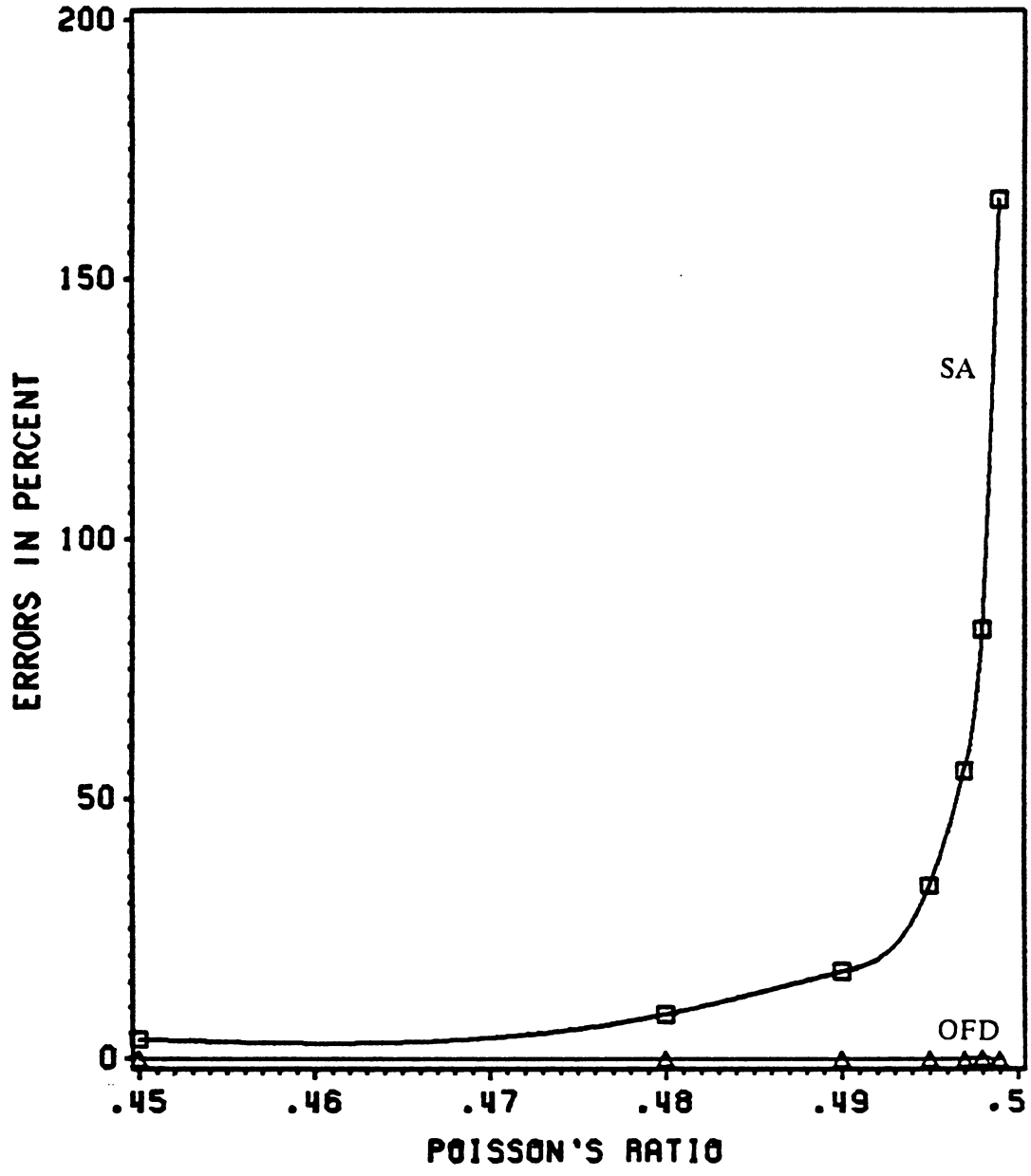

Figure 13. Errors in the SA and OFD approximations for the derivative of strain energy with respect to length of slab modeled with solid elements for varying Poisson's ratio (step size 1 percent)

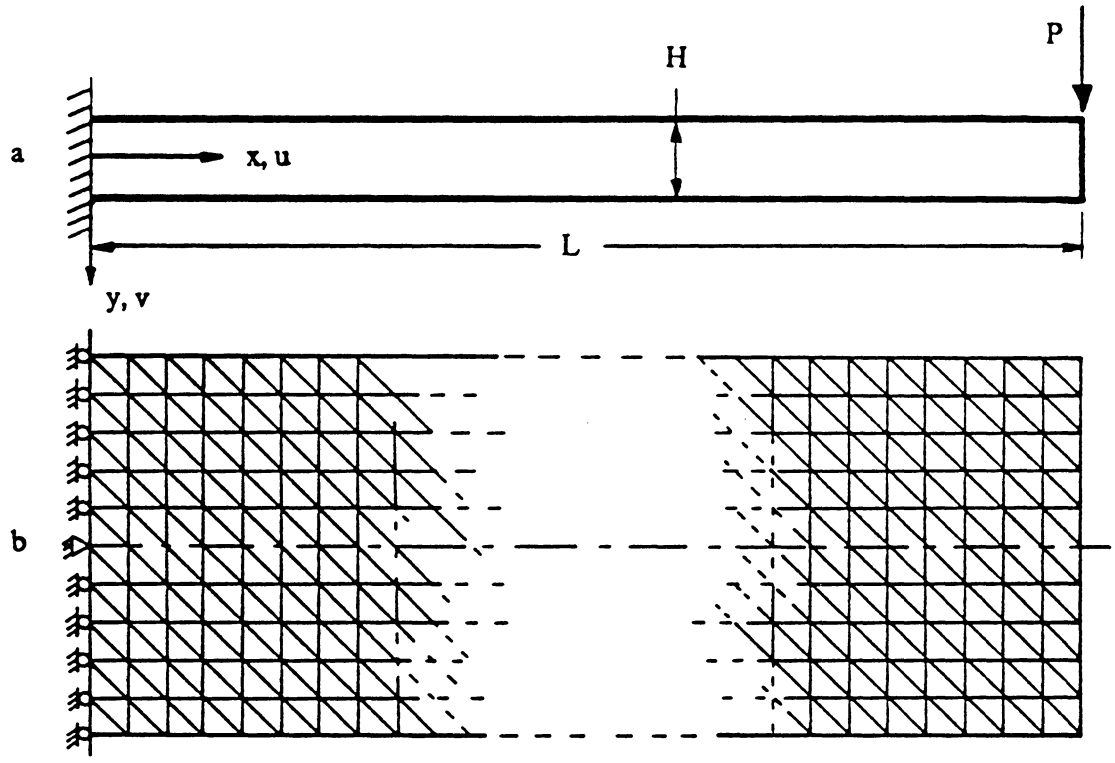

Figure 14. Geometry and loading (a) and finite-element model (b) of cantilever beam modeled by plane stress elements

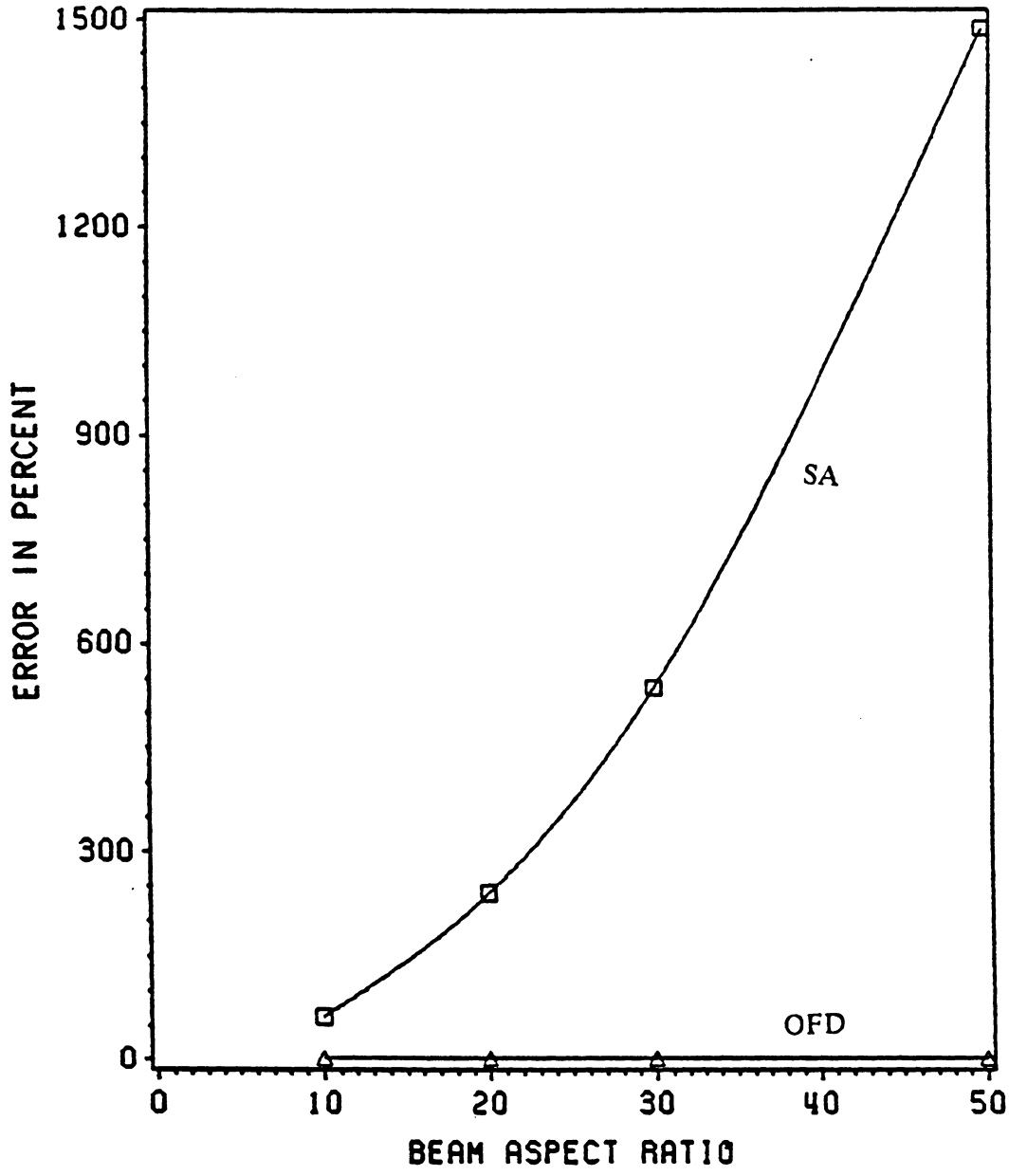

Figure 15. Errors in the SA and OFD approximations for the derivative of vertical tip displacement with respect to length of beam modeled with plane stress triangular elements (step size 1 percent)

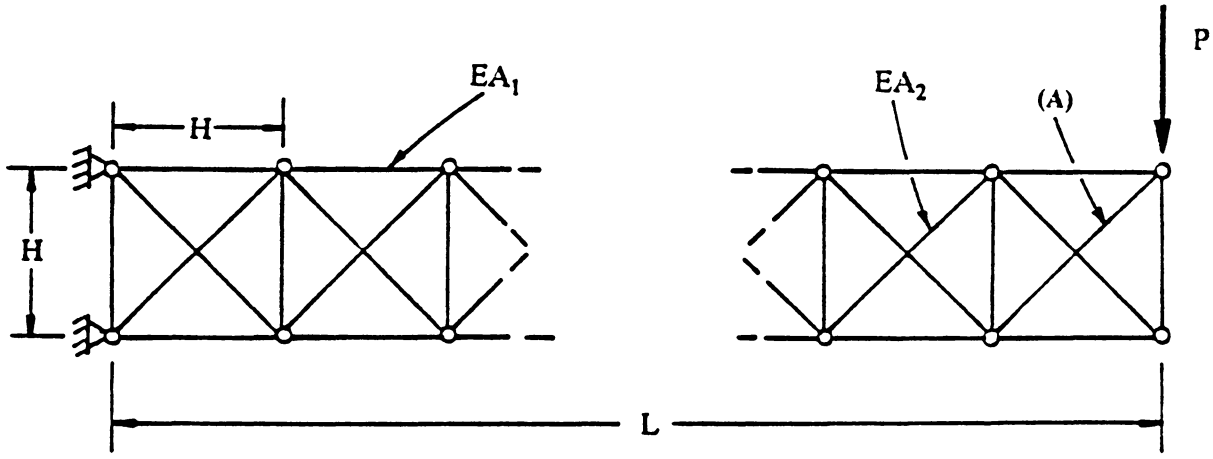

$$A_2 = 125A_1$$

$$L = n \times H \quad (n = 1 \text{ to } 20)$$

Figure 16. Configuration of beam modeled by truss elements

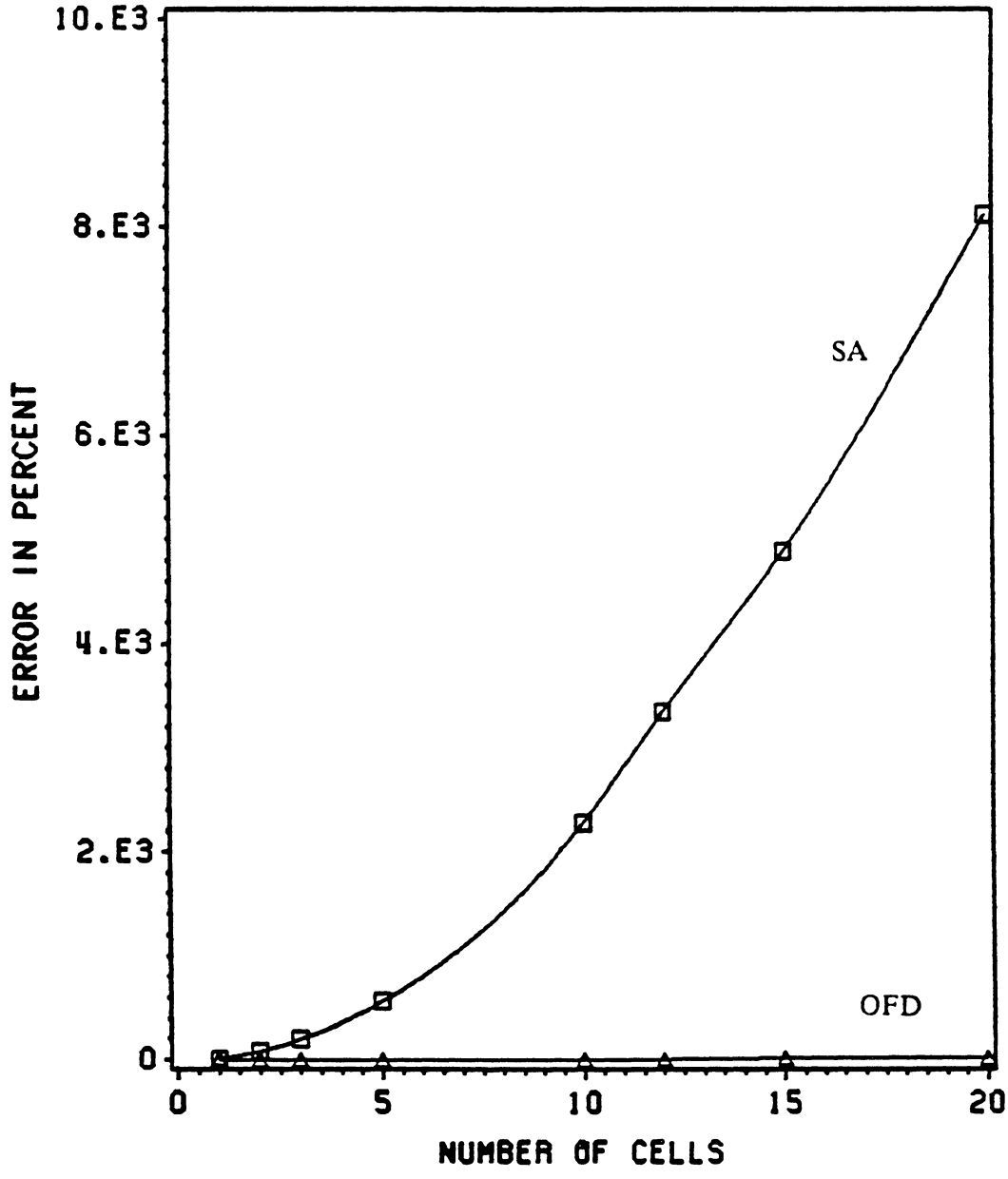

Figure 17. Errors in the SA and OFD approximations for the derivative of strain energy with respect to length of cantilever beam modeled with truss elements (step size 1 percent)

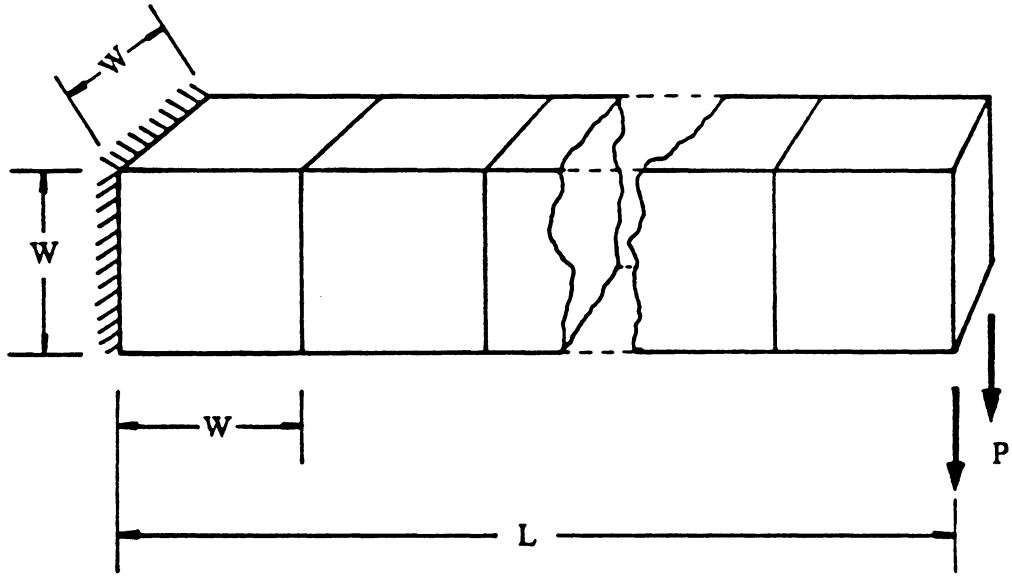

$$L = n \times W \quad (n = 1 \text{ to } 20)$$

Figure 18. Beam modeled by solid elements

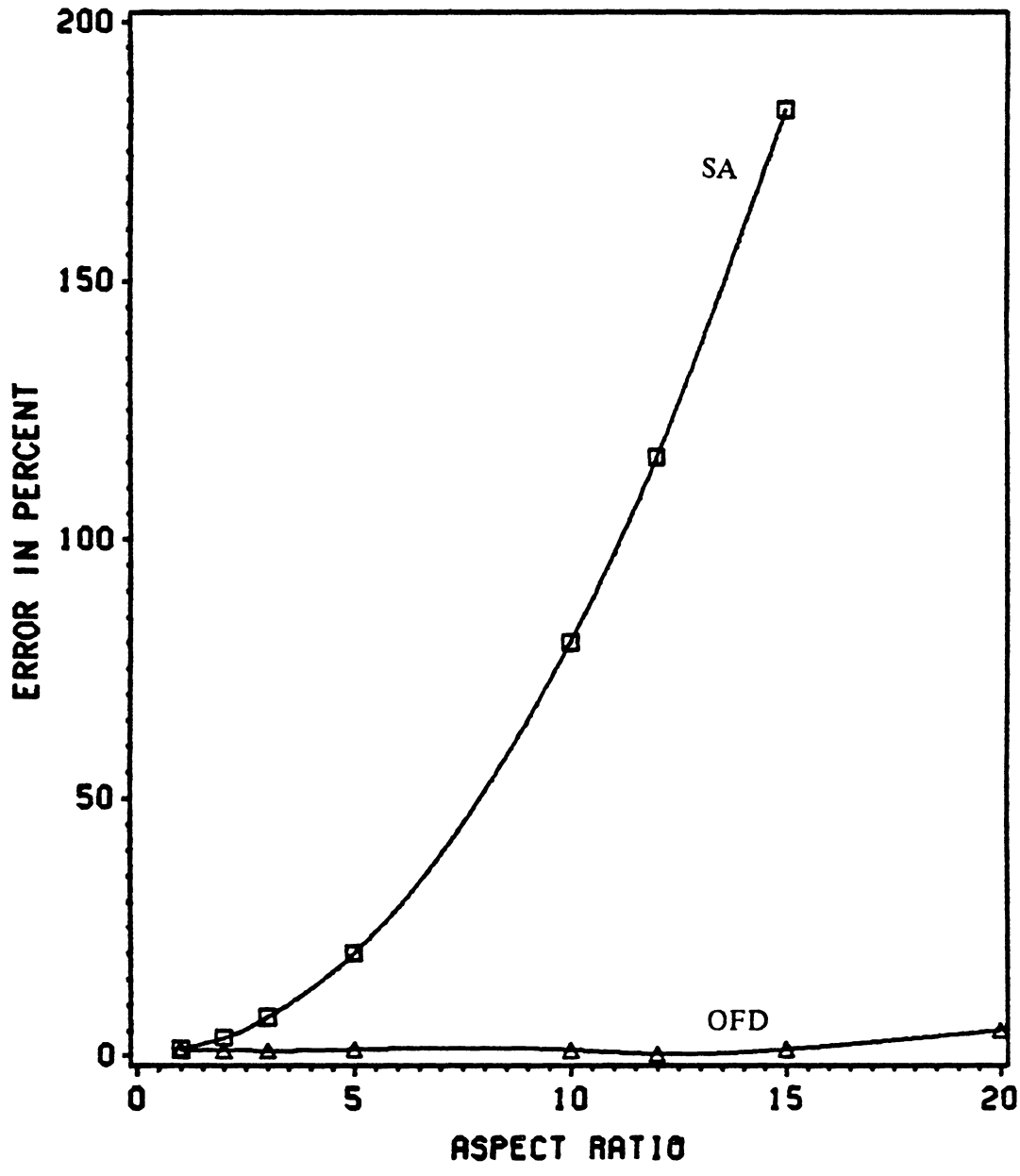

Figure 19. Errors in the OFD and SA approximations for the derivative of strain energy with respect to length of cantilever beam modeled with solid elements (step size 1 percent)

Chapter 3

Error Characterization: Local Error Magnification Index

Local error indices are based on examination of the error contribution of each finite element. They are useful in that they identify the elements that are the worst offenders (i.e., contribute the most to the total error), and permit the analysts to anticipate accuracy problems based on physical characteristics of the finite element model.

3.1 OFD and SA Truncation Errors

The truncation errors associated with the OFD and the SA methods for the forward-difference approximations of the displacement derivatives (Eqs. 2.4 and 2.8) will be denoted as e_{ofd} and e_{sa}, and can be expressed as

$$e_{ofd} = \frac{d^2}{ds^2}\left(K^{-1}p\right)\frac{\Delta s}{2} \qquad 3.1$$

$$e_{sa} = \mathbf{K}^{-1}\left[\frac{d^2\mathbf{p}}{ds^2} - \frac{d^2\mathbf{K}}{ds^2}\mathbf{u}\right]\frac{\Delta s}{2} \qquad 3.2$$

where the second derivatives of $\mathbf{K}^{-1}$, $\mathbf{p}$, and $\mathbf{K}$ are evaluated at a point between s and s + Δs. The errors associated with the strain energy derivatives are similarly given as

$$e_{ofd} = \frac{1}{2}\frac{d^2}{ds^2}(\mathbf{p}^T\mathbf{u})\frac{\Delta s}{2} \qquad 3.3$$

$$e_{sa} = \left[\frac{d^2\mathbf{p}^T}{ds^2}\mathbf{u} - \frac{1}{2}\mathbf{u}^T\frac{d^2\mathbf{K}}{ds^2}\mathbf{u}\right]\frac{\Delta s}{2} \qquad 3.4$$

3.2 Error Magnification Index for Beams

3.2.1 Formulation

In Chapter 2 we showed that even for simple beam structures, the SA method can become very inaccurate as the number of elements increases. The remainder of this chapter presents error indices which can be used to assess the accuracy of the SA method for a given problem. The index can be computed at little extra cost over the cost of obtaining the derivatives, and can point out elements which are responsible for the accuracy problem.

The index is based on the computation of the relative truncation error e_b in the SA approximation of the strain-energy derivatives,

$$e_b = \left|\frac{\dfrac{d^2\mathbf{p}^T}{ds^2}\mathbf{u} - \dfrac{1}{2}\mathbf{u}^T\dfrac{d^2\mathbf{K}}{ds^2}\mathbf{u}}{\dfrac{d\mathbf{p}^T}{ds}\mathbf{u} - \dfrac{1}{2}\mathbf{u}^T\dfrac{d\mathbf{K}}{ds}\mathbf{u}}\right|\left|\frac{\Delta s}{2}\right| \qquad 3.5$$

The numerator is the truncation error for a forward-difference, and the denominator is the strain energy derivative. Both the numerator and denominator can be written as sums of individual element contributions to the truncation error and the strain energy derivative, respectively,

$$e_b = \left| \frac{\sum_{i=1}^{n_e} \left[\frac{d^2 p^{iT}}{ds^2} u^i - \frac{1}{2} u^{iT} \frac{d^2 K^i}{ds^2} u^i \right]}{\sum_{i=1}^{n_e} \left[\frac{dp^{iT}}{ds} u^i - \frac{1}{2} u^{iT} \frac{dK^i}{ds} u^i \right]} \right| \left| \frac{\Delta s}{2} \right| \qquad 3.6$$

where $\mathbf{p}^i$ and $\mathbf{u}^i$ are the load and displacement vectors corresponding to element i, respectively, $\mathbf{K}^i$ is the element stiffness matrix, and n_e is the number of elements in the model. The ratio between the two contributions for a given element (error and strain energy derivative) is a measure of the element contribution to the overall relative error,

$$e_b^i = \left| \frac{\frac{d^2 p^{iT}}{ds^2} u^i - \frac{1}{2} u^{iT} \frac{d^2 K^i}{ds^2} u^i}{\frac{dp^{iT}}{ds} u^i - \frac{1}{2} u^{iT} \frac{dK^i}{ds} u^i} \right| \left| \frac{\Delta s}{2} \right| \qquad 3.7$$

Assuming the stiffness matrix and the load vector depend on s only through the element length L_i, we can replace the derivative with respect to s by a derivative with respect to L_i as

$$\frac{d}{ds} = \frac{d}{dL_i} \frac{dL_i}{ds} \quad \text{and} \quad \Delta L_i = \frac{dL_i}{ds} \Delta s \qquad 3.8$$

Assuming that the relationship between s and L is linear,

$$e_b^i = \left| \frac{\frac{d^2 p^{iT}}{dL_i^2} u^i - \frac{1}{2} u^{iT} \frac{d^2 K^i}{dL_i^2} u^i}{\frac{dp^{iT}}{dL_i} u^i - \frac{1}{2} u^{iT} \frac{dK^i}{dL_i} u^i} \right| \left| \frac{\Delta L_i}{2} \right| = c_b^i \left| \frac{\Delta L_i}{L_i} \right| \qquad 3.9$$

where c_b^i is an error magnification factor called here the error index. The expression for c_b^i is simple when the load does not depend on the design variables.

Case 1: p^i does not depend on s.

For ease of notation, we define r_i, s_i, and t_i:

$$r_i = \frac{w_1^i - w_2^i}{L_i} \tag{3.10}$$

$$s_i = \frac{\theta_1^i + \theta_2^i}{2} \tag{3.11}$$

$$t_i = \theta_2^i - \theta_1^i \tag{3.12}$$

where w_1^i, w_2^i, and θ_1^i, θ_2^i are the nodal translations and rotations of element i (see Fig. 20). Using the stiffness matrix (Fig. 20), the error index c_b^i becomes

$$c_b^i = \left| \frac{72r_i^2 + 72r_is_i + 12s_i^2 + t_i^2}{36r_i^2 + 48r_is_i + 12s_i^2 + t_i^2} \right| \tag{3.13}$$

We simplify Eq. 3.13 further by dividing numerator and denominator by t_i^2, defining

$$\alpha_i = \frac{s_i}{t_i} \tag{3.14}$$

$$\beta_i = \frac{r_i}{t_i} + \frac{s_i}{t_i} \tag{3.15}$$

so that

$$c_b^i = \left| \frac{72\beta_i^2 - 72\alpha_i\beta_i + 12\alpha_i^2 + 1}{36\beta_i^2 - 24\alpha_i\beta_i + 1} \right| \tag{3.16}$$

It is easy to check that α_i is equal to $\frac{\theta_{av}^i}{\Delta\theta^i}$ and β_i is proportional to $\frac{\Delta M^i}{M_{av}^i}$, where θ_{av}^i and M_{av}^i are the average rotation and bending moment in the element while $\Delta\theta^i$ and ΔM^i are the angle and bending moment variations inside the element.

c_b^i in Eq. 3.16 becomes unbounded when α_i goes to infinity, that is, when the rigid body rotation is much larger than the elastic deformation. This is particularly clear for the uniform bending case ($\beta_i = 0$) where Eq. 3.16 becomes

$$c_b^i = 4\left|1 + 3\frac{\theta_1^i\theta_2^i}{(\theta_2^i - \theta_1^i)^2}\right| \qquad 3.17$$

The error index is highest for elements where the ratio of average rotation $\sqrt{\theta_1^i\theta_2^i}$ to deformation $(\theta_1^i - \theta_2^i)$ is highest. As the mesh is refined, the length of each element is decreased and $\theta_1^i\theta_2^i$ converges to a finite value, while $(\theta_2^i - \theta_1^i)$ converges to zero, so that the error grows.

The error index, c_b^i, also becomes unbounded when the denominator of Eq. 3.16 goes to zero; this corresponds to a null contribution of element i to the total strain energy derivative. To avoid a high value of the index for elements which have small strain-energy derivatives, the denominator is replaced by 1 when it is smaller than 1.

Case 2: p^i depends on s.

For distributed loading such as uniform loading, we have to include the terms containing $\frac{dp^{iT}}{dL_i}$ and $\frac{d^2p^{iT}}{dL_i^2}$. For uniform loading with a load p per unit length,

$$p^i = p\frac{L_i}{2}\begin{bmatrix} 1 \\ L_i/6 \\ 1 \\ -L_i/6 \end{bmatrix} \qquad 3.18$$

and the error index becomes

$$c_b^i = \left|\frac{\frac{p_i}{6t_i} + 72\beta_i^2 - 72\alpha_i\beta_i + 12\alpha_i^2 + 1}{2\frac{p_i}{t_i^2}\left[q_i - \frac{t_i}{6}\right] + 36\beta_i^2 - 24\alpha_i\beta_i + 1}\right| \qquad 3.19$$

where

$$q_i = \frac{w_1^i + w_2^i}{2L_i} \tag{3.20}$$

$$p_i = \frac{pL_i^3}{EI} \tag{3.21}$$

For more general loadings, we can compute the load terms by finite differences. The error index becomes

$$c_b^i = \left| \frac{\frac{L_i^3}{EI_i t_i^2} \frac{\Delta^2 p^{iT}}{\Delta L_i^2} u^i - 72\beta_i^2 + 72\alpha_i\beta_i - 12\alpha_i^2 - 1}{2\frac{L_i^2}{EI_i t_i^2} \frac{\Delta p^{iT}}{\Delta L_i} u^i + 36\beta_i^2 - 24\alpha_i\beta_i + 1} \right| \tag{3.22}$$

Based on the examples below, $\frac{\Delta^2 p^{iT}}{\Delta L_i^2} u^i$ can usually be neglected, but $\frac{\Delta p^{iT}}{\Delta L_i} u^i$ should not be omitted. As before, the denominator of Eq. 3.22 is replaced by 1 if it is smaller than 1.

For a well-conditioned function, the error of a forward-difference approximation to the derivative is of the order of the relative step size. For the SA method, the error is magnified by the error magnification index. If we compute the index for all elements in the structure, we obtain a range for the error in the SA method. However, the calculation of the index for every element can be tedious, and it is useful to be able to anticipate the elements with high error magnification indices.

Fig. 21 shows the error magnification index as a function of α_i and β_i for the case where the loads do not depend on the design variables. High values of the magnification factor are associated with large α_i and small β_i. That is, the worst elements have a low ratio of $\frac{\Delta\theta^i}{\theta^i_{av}}$ and a low ratio of $\frac{\Delta M^i}{M^i_{av}}$. When the loads depend on the design variables it is not simple to identify the worst elements, so that more elements need to be evaluated. If the worst element has an error magnification factor which is tolerable, no additional checks are required. Otherwise, it may be possible to reduce

the step size so that the product of $c_0^i \left| \frac{\Delta L_i}{L_i} \right|$ becomes small. If this is not possible because of condition errors, the discretization process should be examined to see if the size of the worst elements could be increased. Because the error magnification index is only an approximation, its correlation with the actual errors was established by the following examples.

3.2.2 Examples

Table 1 presents a summary of some of the cases that were analyzed in this study. The error in the strain energy derivative with respect to the beam length using the SA approximation is presented and compared with an estimate of the error based on the error index. The models of the beams contained 20 equal elements, and the step size of the SA approximation was 1%. Columns 1 and 2 present minimum and maximum values for the error estimate; the numbers in parentheses correspond to the element number for which the index was computed (elements are numbered from left to right). The approximate locations of the elements are presented in the last column in which the geometry and loading are described. The fourth column presents the ratio of the maximum estimated error to the actual error in the strain energy derivative (column 3). The ratio varies between 1.6 and 3.3.

We see that the error index in the worst element is a good conservative indicator of the actual error in the SA strain energy derivative. Similar results were obtained for displacement derivatives.

3.3 Error Magnification Index for Trusses

3.3.1 Formulation

A similar index, expressing the relative contribution of one element to the total truncation error of the SA method for the strain-energy derivative, is derived for plane truss elements. The index is also based on the computation of the relative truncation error e_t in the SA approximation of the strain-energy derivatives,

$$e_t = \left| \frac{\frac{d^2\mathbf{p}^T}{ds^2}\mathbf{u} - \frac{1}{2}\mathbf{u}^T\frac{d^2\mathbf{K}}{ds^2}\mathbf{u}}{\frac{d\mathbf{p}^T}{ds}\mathbf{u} - \frac{1}{2}\mathbf{u}^T\frac{d\mathbf{K}}{ds}\mathbf{u}} \right| \left| \frac{\Delta s}{2} \right| \qquad 3.23$$

Both the numerator and denominator can be written as sums of individual element contributions to the truncation error and the strain energy derivative, respectively. Moreover, we assume loading forces such that $\frac{d\mathbf{p}^T}{ds} = 0$ and $\frac{d^2\mathbf{p}^T}{ds^2} = 0$,

$$e_t = \left| \frac{\sum_{i=1}^{n_e}\left[\frac{1}{2}\mathbf{u}^{iT}\frac{d^2\mathbf{K}^i}{ds^2}\mathbf{u}^i\right]}{\sum_{i=1}^{n_e}\left[\frac{1}{2}\mathbf{u}^{iT}\frac{d\mathbf{K}^i}{ds}\mathbf{u}^i\right]} \right| \left| \frac{\Delta s}{2} \right| \qquad 3.24$$

where $\mathbf{u}^i$ is the displacement vector corresponding to element i, respectively, and $\mathbf{K}^i$ is the element stiffness matrix. The ratio between the two contributions for a given element (error and strain energy derivative) is a measure of the element contribution to the overall relative error,

$$e_t^i = \left| \frac{\frac{1}{2}\mathbf{u}^{iT}\frac{d^2\mathbf{K}^i}{ds^2}\mathbf{u}^i}{\frac{1}{2}\mathbf{u}^{iT}\frac{d\mathbf{K}^i}{ds}\mathbf{u}^i} \right| \left| \frac{\Delta s}{2} \right| \qquad 3.24$$

Eq. 3.24 can be written as

$$e_t^i = c_t^i \left| \frac{\Delta s}{s} \right| \qquad 3.25$$

where c_t^i is the error magnification index and is

$$c_t^i = \left| \frac{\frac{1}{2} u^{iT} \frac{d^2 K^i}{ds^2} u^i}{\frac{1}{2} u^{iT} \frac{dK^i}{ds} u^i} \right| \left| \frac{s}{2} \right| \qquad 3.26$$

Assuming the stiffness matrix depends on s through the element length L_i and the angle α_i between the local and global axes of the element i and the structure (Fig. 22), we can replace the derivatives of K^i with respect to s by derivatives with respect to L_i and α_i as

$$\frac{dK^i}{ds} = \frac{dK^i}{dL_i} \frac{dL_i}{ds} + \frac{dK^i}{d\alpha_i} \frac{d\alpha_i}{ds} \qquad 3.27$$

$$\frac{d^2K^i}{ds^2} = \frac{d^2K^i}{dL_i^2} \left[\frac{dL_i}{ds} \right]^2 + \frac{d^2K^i}{d\alpha_i^2} \left[\frac{d\alpha_i}{ds} \right]^2 + 2 \frac{d^2K^i}{d\alpha_i dL_i} \frac{d\alpha_i}{ds} \frac{dL_i}{ds} + \frac{dK^i}{dL_i} \frac{d^2L_i}{ds^2} + \frac{dK^i}{d\alpha_i} \frac{d^2\alpha_i}{ds^2} \qquad 3.28$$

The stiffness matrix K^i corresponding to Fig. 22 is written as

$$K = \frac{EA}{L_i} \begin{bmatrix} c^2 & cs & -c^2 & -cs \\ cs & s^2 & -cs & -s^2 \\ -c^2 & -cs & c^2 & cs \\ -cs & -s^2 & cs & s^2 \end{bmatrix} \qquad 3.29$$

where $c = \cos \alpha_i$ and $s = \sin \alpha_i$. The vector of nodal displacements of the element (see Fig. 22) is

$$\mathbf{u}^i = \begin{bmatrix} u_1^i \\ v_1^i \\ u_2^i \\ v_2^i \end{bmatrix} \qquad 3.30$$

The derivatives of K in Eqs. 3.27 and 3.28 are evaluated in the local coordinate system of the truss element (see Fig. 22) in which the displacement field becomes

$$u_j^{i\prime} = u_j^i \cos\alpha_i + v_j^i \sin\alpha_i \qquad 3.31$$

$$v_j^{i\prime} = -u_j^i \sin\alpha_i + v_j^i \cos\alpha_i \qquad 3.32$$

for j = 1 and 2. We define the strain and rotation of the truss i as

$$\varepsilon_i = \frac{u_2^{i\prime} - u_1^{i\prime}}{L_i} \qquad 3.33$$

$$\omega_i = \frac{v_2^{i\prime} - v_1^{i\prime}}{L_i} \qquad 3.34$$

Eq. 3.26 becomes

$$c_t^i = \left| \frac{2 + 2(\beta_i^2 - 1)\gamma_i^2 - 4\beta_i\gamma_i + \Theta_2}{2\beta_i\gamma_i - 1} \frac{dL_i}{ds} \right| \left| \frac{s}{2L_i} \right| \qquad 3.35$$

where $\beta_i = \frac{\omega_i}{\varepsilon_i}$ and $\gamma_i = (L_i \frac{d\alpha_i}{ds}) / \frac{dL_i}{ds}$, and Θ_2 contains second order terms

$$\Theta_2 = 2\beta_i \frac{L_i^2 \frac{d^2\alpha_i}{ds^2}}{\left[\frac{dL_i}{ds}\right]^2} - \frac{L_i \frac{d^2 L_i}{ds^2}}{\left[\frac{dL_i}{ds}\right]^2} \qquad 3.36$$

In the following example presented in the text, the second order terms could be neglected without loss of accuracy. Neglecting second order effects, the index becomes

$$c_t^i = \left| \frac{1 + (\beta_i^2 - 1)\gamma_i^2 - 2\beta_i\gamma_i}{2\beta_i\gamma_i - 1} \frac{dL_i}{ds} \right| \left| \frac{s}{L_i} \right| \qquad 3.37$$

where β_i is the ratio of the truss element rotation to the element strain, and γ_i is the ratio of truss rotation to truss extension due to the change in the shape variable s (see Fig. 23). The index shows that the error is high when β_i and γ_i are large. This occurs for elements that have large rigid body rotation as compared to strain and where the design variable change causes large rotations of the element as compared to change in length.

Computation of c_t^i for each element might be difficult if we use black-box finite element programs. We should then compute it for the elements we judge most critical. These elements can be chosen on the bases of γ_i, β_i , and their respective contribution to the total strain energy derivative of the structure.

3.3.2 Example

The truss structure of Fig. 16 is used to demonstrate the use of the index. The index c_t^i was computed for diagonal element A, Fig. 16, because this element had the largest γ_i. Fig. 24 presents the ratio of the index $c_t^i \left| \frac{\Delta s}{s} \right|$ to the error in the SA prediction of the strain-energy derivative (for a step size of 1 percent) versus the number of cells in the model. The ratio was close to 2 for any number of cells, indicating that c_t^i is a conservative index.

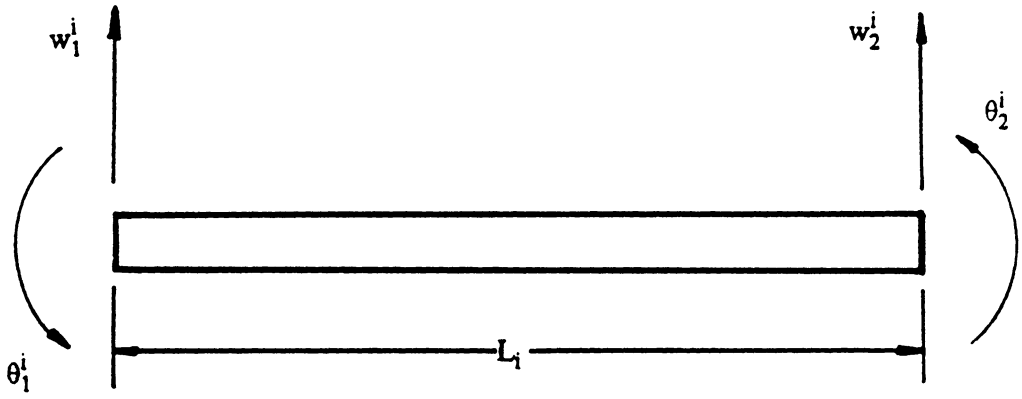

$$\mathbf{u}^i = \begin{bmatrix} w_1^i \\ \theta_1^i \\ w_2^i \\ \theta_2^i \end{bmatrix} \qquad \mathbf{K}^i = \frac{EI}{L_i^3} \begin{bmatrix} 12 & 6L_i & -12 & 6L_i \\ 6L_i & 4L_i^2 & -6L_i & 2L_i^2 \\ -12 & -6L_i & 12 & -6L_i \\ 6L_i & 2L_i^2 & -6L_i & 4L_i^2 \end{bmatrix}$$

Figure 20. Sign convention for beam finite element

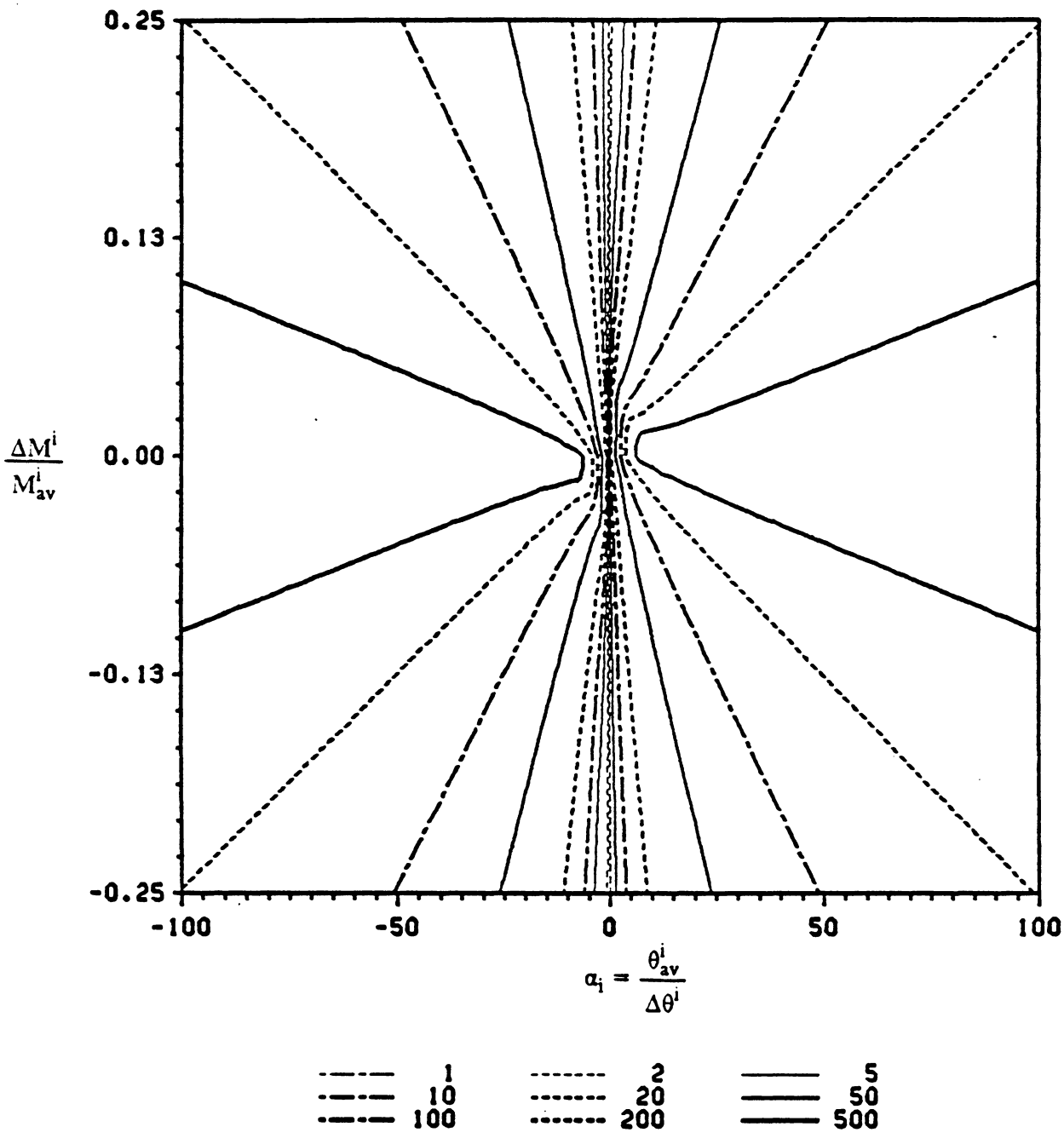

Figure 21. Contour of the error magnification index

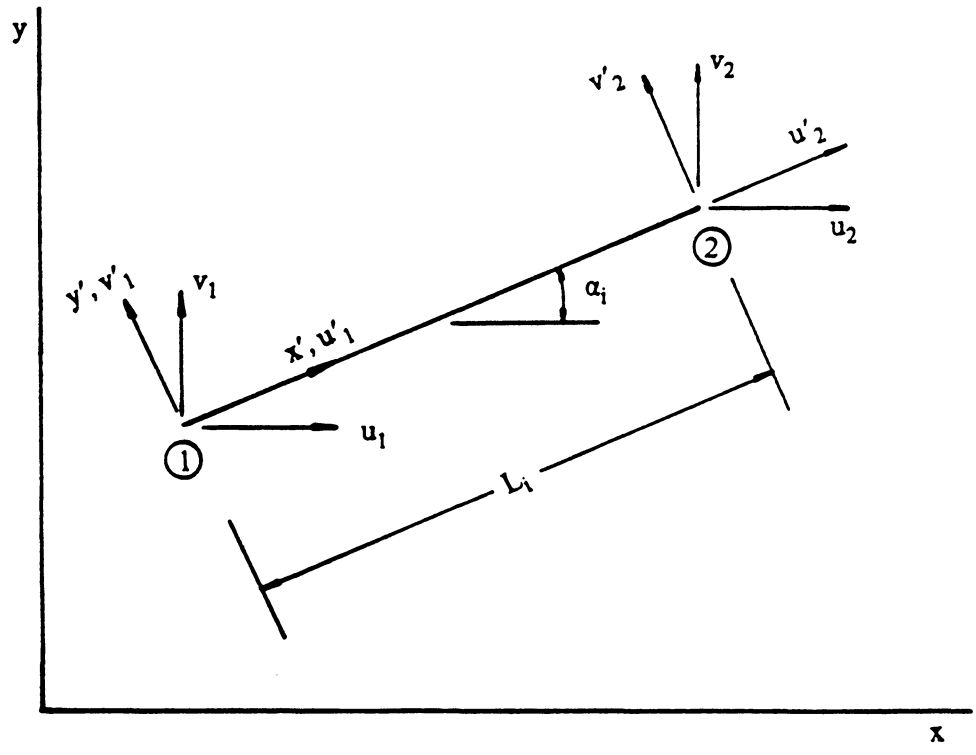

Figure 22. Definitions for local and global axes for truss elements

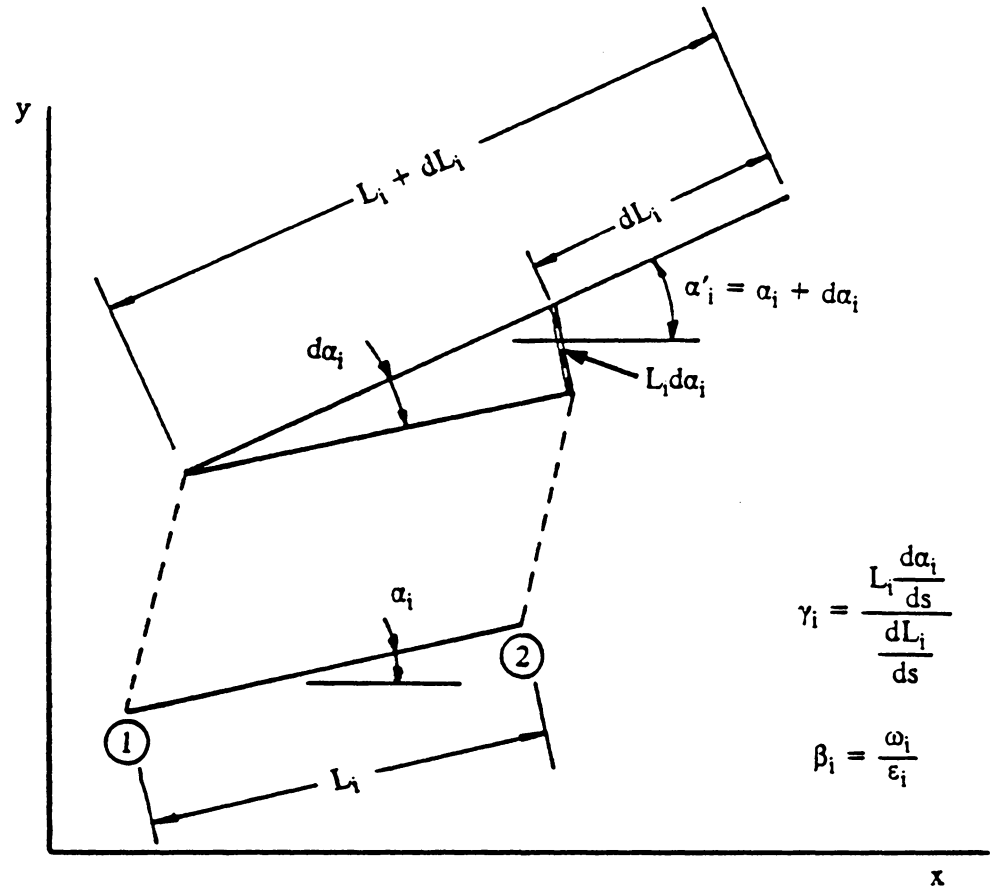

Figure 23. Definitions for β_i and γ_i

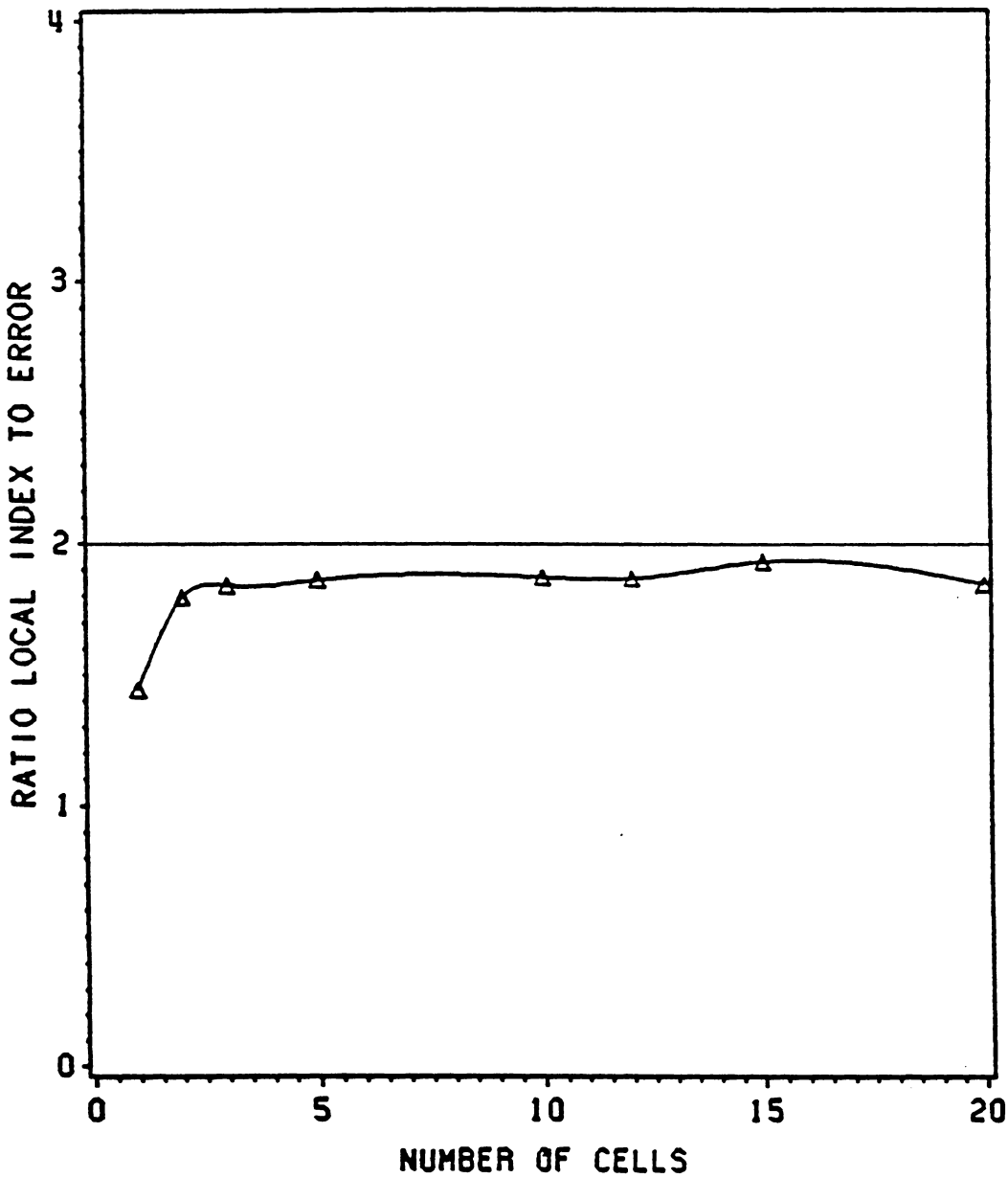

Figure 24. Ratio of the local index computed in the diagonal element (A) of the truss Fig. 16 to the error in SA approximation of strain-energy derivative with respect to length of beam

Table 1. Error estimate based on index compared to actual error in the SA approximation of the strain energy derivative for different beam cases

lowest $100 \times C\frac{\Delta L}{L}$	maximum $100 \times C\frac{\Delta L}{L}$	relative error percent	$\frac{\max C\frac{\Delta L}{L}}{\text{error}}$	Geometry
4 (1)	4560 (20)	1550	2.9	
4 (1)	1200 (20)	618	1.9	
4 (1)	533 (20)	324	1.6	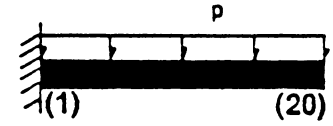
4 (1)	931 (20)	399	2.3	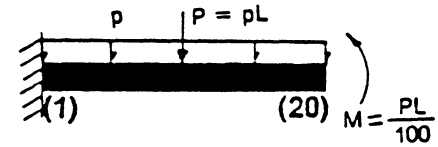
10 (10)	847 (1)	380	2.2	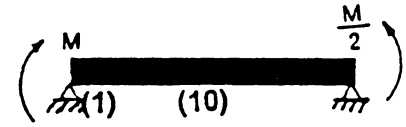
4 (10)	200 (1)	119	1.7	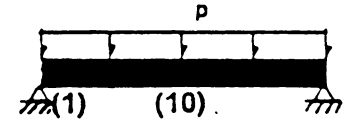
4 (1)	240 (20)	73	3.3	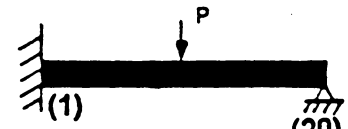
4 (1)	75 (5)	41	1.8	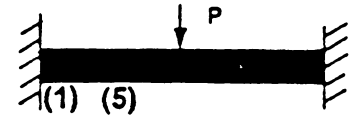

( ) element number in which the index was computed.

Chapter 4

Error Characterization: Global Error Index

Deriving a local error index for each finite element type would require a lot of work and may be difficult to implement. Moreover, the error magnification indices give only local information on the total error, and in some cases the interpretation of the results might be difficult. Therefore a global error index which is easier to implement was derived.

4.1 Formulation

With some algebraic manipulations, we can rewrite the OFD approximations, Eq. 2.4, for a forward-finite difference as

$$\left[\frac{\Delta \mathbf{u}}{\Delta s}\right]_{ofd} = \mathbf{K}_{+}^{-1}\left[\frac{\Delta \mathbf{p}}{\Delta s} - \frac{\Delta \mathbf{K}}{\Delta s}\mathbf{u}\right] \qquad 4.1$$

where $\mathbf{K}_+^{-1} = \mathbf{K}^{-1}(s + \Delta s)$. Eq. 4.1 implies that $\left[\frac{\Delta \mathbf{u}}{\Delta s}\right]_{ofd}$ can be interpreted as the displacements of the perturbed structure due to the pseudo-load vector. Ignoring condition errors, we write a relation between the OFD and SA errors in the strain energy derivatives as

$$\frac{dV}{ds} = \left[\frac{\Delta V}{\Delta s}\right]_{ofd} + e_{ofd} = \left[\frac{\Delta V}{\Delta s}\right]_{sa} + e_{sa} \tag{4.2}$$

Then using Eqs. 4.2, 4.1, and 2.11, we express $\frac{dV}{ds}$ as

$$\frac{dV}{ds} = \left[\frac{\Delta V}{\Delta s}\right]_{sa} + e_{ofd} + \frac{1}{2}\mathbf{p}^T\left[\mathbf{K}_+^{-1} - \mathbf{K}^{-1}\right]\left[\frac{\Delta \mathbf{p}}{\Delta s} - \frac{\Delta \mathbf{K}}{\Delta s}\mathbf{u}\right] \tag{4.3}$$

For small Δs, $\mathbf{K}_+^{-1}$ is expanded as

$$\mathbf{K}_+^{-1} = (\mathbf{K} + \Delta \mathbf{K})^{-1} = (\mathbf{I} + \mathbf{K}^{-1}\Delta \mathbf{K})^{-1}\mathbf{K}^{-1} \cong (\mathbf{I} - \mathbf{K}^{-1}\Delta \mathbf{K} + \mathbf{K}^{-1}\Delta \mathbf{K}\mathbf{K}^{-1}\Delta \mathbf{K} - ...)\mathbf{K}^{-1} \tag{4.4}$$

and Eq. 4.3 becomes

$$\frac{dV}{ds} = \left[\frac{\Delta V}{\Delta s}\right]_{sa} + e_{ofd} + \sum_{i=1}^{\infty} e_i \tag{4.5}$$

where e_i is obtained as a solution to the iterative problem

$$e_i = \frac{1}{2}\mathbf{p}^T\mathbf{u}_i \tag{4.6}$$

$$\mathbf{u}_i = -\mathbf{K}^{-1}\Delta \mathbf{K}\mathbf{u}_{i-1} \qquad \text{with} \qquad \mathbf{u}_o = \left[\frac{\Delta \mathbf{u}}{\Delta s}\right]_{sa} \tag{4.7}$$

If the series e_i does not converge, or if its terms are large compared to $\left[\frac{\Delta V}{\Delta s}\right]_{sa}$, we should expect large errors using the SA method. If the first few terms are not excessively large, they can be used to improve the accuracy of the SA method. Defining $\left[\frac{\Delta V}{\Delta s}\right]^n$ as

$$\left[\frac{\Delta V}{\Delta s}\right]^n = \left[\frac{\Delta V}{\Delta s}\right]_{sa} + \sum_{i=1}^{n} e_i \qquad \text{with} \qquad \left[\frac{\Delta V}{\Delta s}\right]^0 = \left[\frac{\Delta V}{\Delta s}\right]_{sa} \tag{4.8}$$

each term in the series requires the same effort as the computation of one derivative using the SA method. It is still less expensive to use the SA method with a few correction terms than to use the OFD method. However, instead of using this approach, a central-finite difference computation could possibly give us better accuracy at a lower cost.

Another error index is based on the SA improvement formula

$$E^{lmn} = \left| \frac{\left[\frac{\Delta V}{\Delta s}\right]^l - \left[\frac{\Delta V}{\Delta s}\right]^m}{\left[\frac{\Delta V}{\Delta s}\right]^n} \right| \qquad 4.9$$

The following strategy is proposed for using this index with the SA method, if the nature of the problem, a local index, or other indications point to possible accuracy problems:

1. Calculate the term e_1 and calculate E^{100}. If E^{100} is substantially smaller than the tolerable error, the SA truncation error is likely to be small, and the accuracy can be improved by using $\left[\frac{\Delta V}{\Delta s}\right]^1$ instead of $\left[\frac{\Delta V}{\Delta s}\right]_{sa}$.

2. If E^{100} is not small, calculate e_2 and E^{210}. If E^{210} is much smaller than E^{100}, the series converges fast and even though $\left[\frac{\Delta V}{\Delta s}\right]_{sa}$ has large error, $\left[\frac{\Delta V}{\Delta s}\right]^2$ is likely to be a good approximation. In this case E^{202} will be a good approximation of the relative difference of the SA method from the OFD method, and could be used for estimating the SA error. Still, it may be safer and even more efficient to switch to the central difference or the OFD approximations.

3. If both E^{100} and E^{210} are not small and the step size cannot be reduced because of condition errors, the forward-difference SA method should not be used.

The expressions for the errors in the displacement derivatives of the SA method are identical to Eqs. 4.3-4.7 except that the coefficient $\frac{1}{2}\mathbf{p}^T$ is removed from the equations, and e_i becomes $\mathbf{u}_i$ (Eq. 4.6).

4.2 Examples

Truss Structure We first applied the global index to our truss structure, Fig. 16. Fig. 25 presents the errors computed with respect to the OFD method of the strain-energy derivative with respect to the beam length using the SA method for a step size of 1 percent and the SA improvement formula (Eq. 4.8) versus the number of cells in the model (1, 2, 5, 10, 12, and 20 cells). The triangles correspond to the errors of the SA method (Eq. 2.8), and the squares, diamonds, circles, plus signs, and stars correspond to Eq. 4.8 using 1 to 5 terms (i.e., e_1 to e_5), respectively. The results show that for small aspect ratios (corresponding to short beams with 1 to 3 cells), the errors tend to decrease as we increase the number of terms in the improved estimation of the strain-energy derivative. However, for 10, 12, and 20 cells the method diverges even if we keep increasing the number of correction terms in Eq. 4.8. This implies that for the step size used, we will not be able to predict the derivatives accurately using the SA method (using forward-finite difference Eq. 2.8) for more than 5 cells.

Table 2 presents the global index; E^{100} and E^{210} (second and third columns) are presented for the truss structures containing 1, 2, 5, 10, and 20 cells. The table is divided into 3 regions (by horizontal lines) corresponding to the 3 cases described in the preceding section. For 1 cell E^{100} (second column) indicates that the SA method is able to predict a derivative with a reasonable error (17 percent), and the last two columns show that we can still improve on the accuracy of the SA method by using one or two additional terms. For 2 and 5 cells, E^{210} (third column) is small, implying that E^{202} (fourth column) will be a good approximation to the relative difference between the SA method and the OFD method (fifth column) for the strain-energy derivative, and that $\left[\frac{\Delta V}{\Delta s}\right]^1$ is an improved approximation to $\frac{dV}{ds}$. For 10 and 20 cells, E^{210} is large, and E^{202} is no longer a good approximation to the SA errors.

Solid Beam Similar results are found for the solid beam of Fig. 18. Table 3 presents a summary of the results for step sizes of 10 and 1 percent. In this example the first column is the aspect ratio

for the beam. For the 10 percent case the SA cannot predict the derivatives with an error of less than 20 percent. For 1, 2, and 5 cells, we can improve on the SA accuracy by computing additional terms; however, for 5 cells the convergence is very slow, and 5 terms are needed in the improvement formula in order to decrease the error to a reasonable level. For aspect ratios of 10 and 20, the method diverges. For 1 percent step size, the SA method obtains the derivatives with reasonable errors for the beams with an aspect ratio of 5 or less. The method still converges for aspect ratios of 10 and 20, and additional terms will decrease the errors.

Frame Structure Finally, we analyzed a cantilever beam (Fig. 26) made of square cells modeled with beam elements for the flanges and truss elements for the webs. In this example, we are interested in the effect on the accuracy of the SA method (for a step size of 1 percent) of both the beam aspect ratio and different discretizations of the flanges. The number of cells was varied from 1 to 20, changing the aspect ratio of the beam from 1 to 20, and the flanges were discretized using one-beam and five-beam elements per flange in each cell. Table 4 summarizes the results; for one-beam per flange case, the SA method gives us derivatives having an error less than 13 percent for the structure containing 1 or 2 cells. For 5 and 10 cells, the SA method fails to obtain accurate derivatives (errors > 58 percent); however, additional terms bring the errors down to 1 percent. Very large error is obtained for the 20 cells case. For five-elements per flange, the SA method had large errors for all of the structures tested (larger than 33 percent). For 1 to 5 cells, we can still improve on the SA accuracy; however, the convergence is very slow for 5 cells. For 10 and 20 cells, the method diverges and the errors increase as the number of terms is increased.

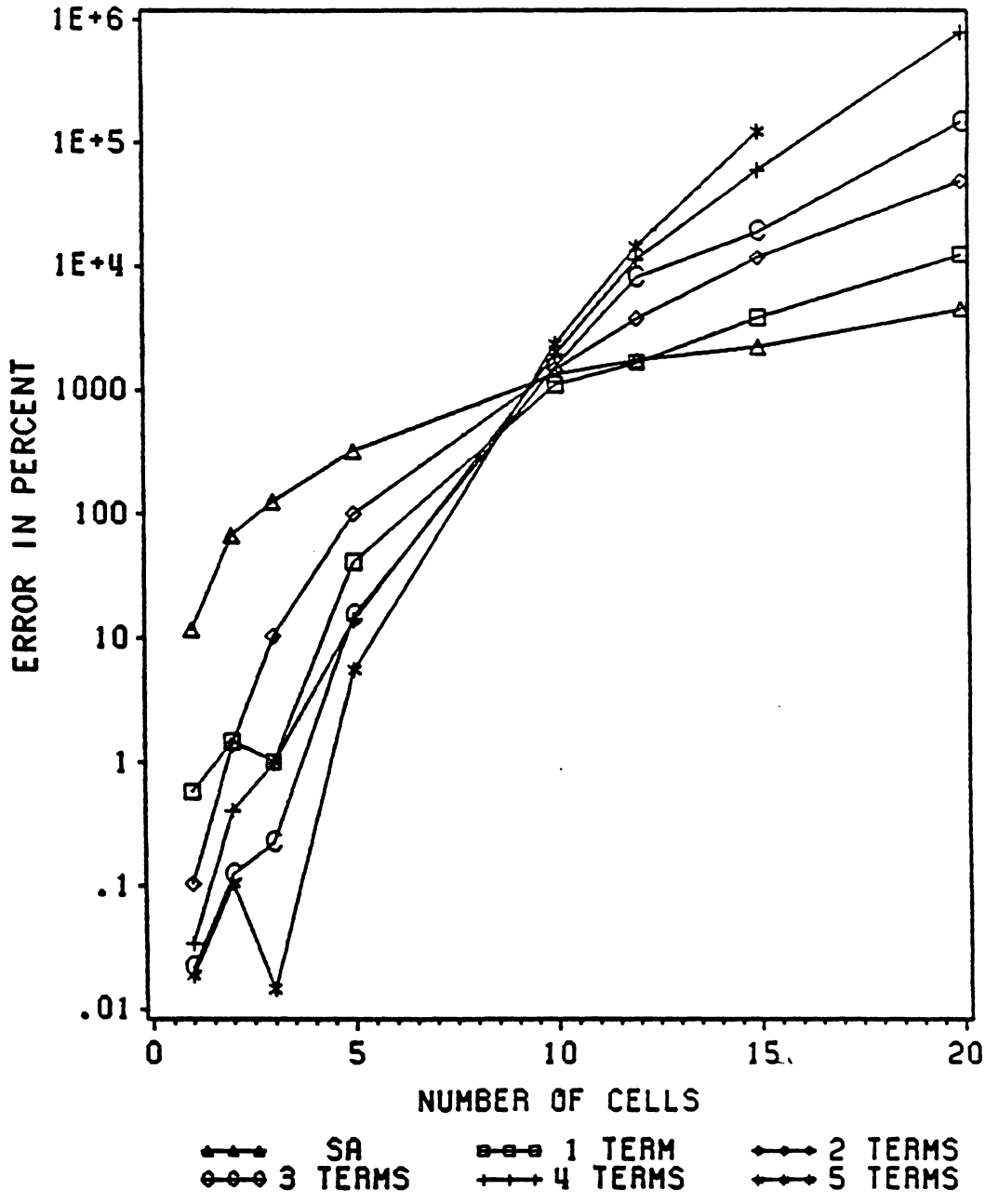

Figure 25. Errors (with respect to the OFD method) of the SA method and the SA improvement formula with 1, 2, 3, 4, and 5 terms for the strain-energy derivatives (step size 1 percent) for truss model

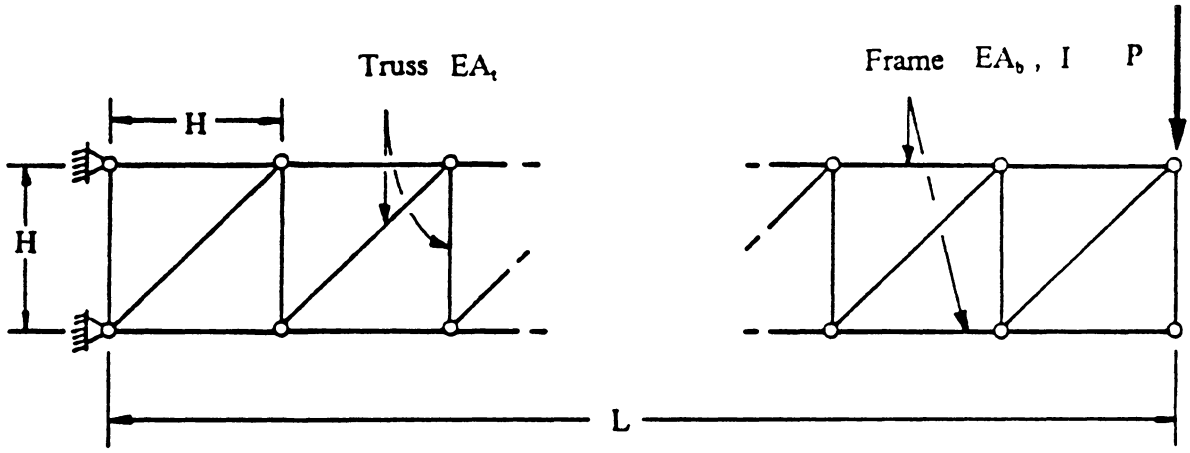

$$L = n \times H \quad (n = 1 \text{ to } 20)$$

$$EA_t = 25 \times EA_b$$

$$I = \frac{5}{16} \times A_b^2$$

Figure 26. Geometry, loading, and finite-element model of cantilever beam modeled by frame and truss elements

Table 2. Global index for the truss structure of Fig. 16 (step size 1 percent)

Number of Cells	E^{100}	E^{210}	E^{202}	Relative Errors WRT OFD of $\left[\frac{\Delta V}{\Delta s}\right]_{sa}$	$\left[\frac{\Delta V}{\Delta s}\right]^1$	$\left[\frac{\Delta V}{\Delta s}\right]^2$
1	.19	.01	.16	.165	.008	.001
2	5.7	.02	.85	.854	.026	.023
5	1.4	.38	5.8	5.64	.661	1.07
10	1.7	1.9	.13	22.2	14.3	25.3
20	3.8	13.	.90	69.4	190.	720.

Table 3. Global index for the solid beam of Fig. 18 (step size of 10 and 1 percent)

Aspect Ratio	E^{100}	E^{210}	E^{202}	Relative Errors WRT OFD of $\left[\frac{\Delta V}{\Delta s}\right]_{sa}$	$\left[\frac{\Delta V}{\Delta s}\right]^1$	$\left[\frac{\Delta V}{\Delta s}\right]^2$	
1	.23	.04	.21	.221	.041	.008	
2	.50	.12	.38	.406	.112	.033	
5	2.4	1.4	49.	1.79	.116	.998	10 percent
10	3.2	8.6	.84	6.74	11.4	37.9	
20	9.7	92.	.99	27.7	230.	2230.	
1	.03	.00	.02	.025	.001	.0002	
2	.05	.00	.05	.047	.002	.0006	
5	.26	.01	.21	.212	.009	.001	1 percent
10	4.0	.01	.80	.804	.020	.019	
20	1.5	.2	4.9	3.56	.187	.356	

Table 4. Global index for the frame structure of Fig. 26 one-element and five-elements per flange (step size 1 percent)

Number of Cells	E^{100}	E^{210}	E^{202}	Relative Errors WRT OFD of $\left[\frac{\Delta V}{\Delta s}\right]_{sa}$	$\left[\frac{\Delta V}{\Delta s}\right]^1$	$\left[\frac{\Delta V}{\Delta s}\right]^2$	
1	.06	.00	.06	.061	.003	.0001	
2	.14	.01	.13	.128	.006	.0005	one-beam
5	1.3	.03	.58	.581	.023	.001	element
10	1.9	.13	2.4	2.17	.018	.014	per flange
20	1.4	.05	3.8	8.70	1.74	2.615	
1	.48	.02	.33	.337	.018	.003	
2	4.1	.08	.81	.810	.034	.019	five-beam
5	1.4	.24	6.9	3.98	.211	.496	element
10	1.5	1.1	.67	15.0	5.89	9.39	per flange
20	2.8	6.7	.80	59.7	103.	289.	

Chapter 5

Concluding Remarks

The semi-analytical method, widely used for calculating derivatives of static response with respect to design variables for structures modeled by finite elements, was studied in this research. It was demonstrated that the method can have serious accuracy problems for shape design variables in structures modeled by beam, plate, truss, frame, and solid elements.

Local and global indices were developed to test the accuracy of the SA method. The local indices provide insight into the problem of large errors for the SA method. Error magnification indices were developed for beam and plane truss structures, and several examples showing the severity of the problem were presented. The accuracy problem was shown, for beam structures, to be associated with high ratios of rigid body rotation to elastic deformation. For truss elements, the errors were due to high ratios of rigid body rotation to axial deformation, where ratios are computed for the deformation field and change in shape field.

The global index provides us with a general method for checking the accuracy of the SA method for any type of model. It characterizes the difference in errors between the OFD and the SA

methods. Moreover, a method improving the accuracy of the SA method (when it is possible) was provided. Examples were presented showing the use of the global index.

References

[1] Adelman, H.M. and Haftka, R.T., "Sensitivity Analysis For Discrete Structural Systems," AIAA Journal, Volume 24, No 5, May 1986, pp. 823-831.

[2] Sensitivity Analysis Symposium, "Sensitivity Analysis in Engineering," NASA Langley, NASA Conference Publication 2457, Sept 9-10 1986.

[3] Dopker, B. and Choi, K.K., "A Study of Solution Algorithms for Shape Design Sensitivity Analysis on a Supermini Computer with an Attached Array Processor," Engineering with Computers, (to be published).

[4] Haug, E.J., Choi, K.K., and Komkov, V., Design Sensitivity Analysis of Structural Systems, Academic Press, 1986.

[5] Haug, E.J. and Choi, K.K., "Material Derivative Methods for Shape Design Sensitivity Analysis," The Optimum Shape: Automated Structural Design, Edited by J.A. Bennet and M.E. Botkin, General Motors Symposia Series, Plenum Press, 1986, pp 29-60.

[6] Dopker, B. and Choi, K.K., "Sizing and Shape Design Sensitivity Analysis using a Hybrid Finite Element Code," Finite Elements in Analysis and Design (to be published).

[7] Dems, K. and Mróz, Z., "Variational Approach by Means of Adjoint System to Structural Optimization and Sensitivity Analysis-I," International Journal of Solids and Structures, Vol. 19, No 8, pp. 677-692, 1983.

[8] Dems, K. and Mróz, Z., "Variational Approach by Means of Adjoint System to Structural Optimization and Sensitivity Analysis-II," International Journal of Solids and Structures, Vol. 20, No 6, pp. 527-552, 1984.

[9] Haftka, R.T. and Mróz, Z., "First- and Second-Order Sensitivity Analysis of Linear and Nonlinear Structures," AIAA Journal, Vol. 24, No 7, pp 823-832, 1986.

[10] Dems, K. and Haftka, R.T. "Two Approaches for Sensitivity Analysis for Shape Variation of Structures," Mechanics of Structures and Machines, (to be published).

[11] Barthelemy, B., Haftka, R.T., and Cohen, G.E., "Physically Based Sensitivity Derivatives for Structural Analysis Programs," Computational Mechanics, (to be published).

[12] Nagendra, G.K. and Fleury, C., "Sensitivity and Optimization of Composite Structures Using MSC/NASTRAN," NASA Langley, NASA Conference Publication 2457, pp.147-159, Sept 9-10 1986.

[13] Wallerstein, D.V., "Design Enhancement Tools in MCS/NATRAN," NASA CP-2327, pp 505-526, 1984.

[14] Camarda, C.J. and Adelman, H.M. "Implementation of Static and Dynamic Structure Sensitivity Derivative Calculations in the Finite-Element-Based Engineering Analysis Language System (EAL)," NASA TM-85743, 1984.

[15] Fleury, C. "Computer Aided Optimal Design of Elastic Structures," Computer Aided Optimal Design: Structural and Mechanical Systems, Edited by Carlos A. Mota Soares, NATO ASI Series, Series F: Computer and Systems Sciences, Vol. 27, pp. 831-900, 1987.

[16] Cheng Ghengdong and Liu Yingwei, "New Computation Scheme of Sensitivity Analysis," paper presented at the First World Congress on Computational Mechanics, Austin Texas, Sept 22-26 1986.

[17] Barthelemy, B., Chon, C.T., and Haftka, R.T., "Sensitivity Approximation of the Static Structural Response," paper presented at th First World Congress on Computational Mechanics, Austin, Texas, Sept 6-8, 1986.

[18] Gill, P.E., Murray, W., Saunders, M.A., and Wright, M.H., "Computing Forward-Difference Intervals for Numerical Optimization," SIAM Journal on Scientific and Statistical Computing, Vol. 4, No. 2, June 1983, pp. 310-321.

[19] Iott, J., Haftka, R.T., and Adelman, H.M. "Selecting Step Sizes in Sensitivity Analysis by Finite Difference," NASA TM-86383, 1985.

[20] Barthelemy, B., Chon, C.T., and Haftka, R.T., "Accuracy Problem Associated with Semi-Analytical Derivatives of Static Response," paper submitted to Finite Elements in Analysis and Design.

[21] Whetstone, W.D.: EISI-EAL Engineering Analysis Language Reference Manual - EISI-EAL System Level 2091. Engineering Information Systems, Inc., July 1983.

[22] Shames, I.H. and Dym, C.L., "Energy and Finite Element Methods in Structural Mechanics," McGraw-Hill, pp. 55-58, 1985.

The vita has been removed from the scanned document